Validation of glacial-interglacial rainfall variations in southwest Sulawesi using Mg/Ca and $\delta^{18}O$ in speleothems

Alena K. Kimbrough[1,2*], Michael K. Gagan[1,2,3], Gavin B. Dunbar[4], Wahyoe S. Hantoro[5,2], Chuan-Chou Shen[6,7], Hsun-Ming Hu[6,7], Hai Cheng[8,9], R. Lawrence Edwards[10], Hamdi Rifai[11], Bambang W. Suwargadi[5]

[1] Research School of Earth Sciences, The Australian National University, Acton, ACT 2601, Australia
[2] School of Earth, Atmospheric and Life Sciences, University of Wollongong, Wollongong, NSW 2522, Australia
[3] School of Earth and Environmental Sciences, The University of Queensland, Brisbane, QLD 4072, Australia
[4] Antarctic Research Centre, Victoria University of Wellington, Wellington 6140, New Zealand
[5] Research Center for Geotechnology, Indonesian Institute of Sciences, Bandung 40135, Indonesia
[6] High-Precision Mass Spectrometry and Environment Change Laboratory (HISPEC), Department of Geosciences, National Taiwan University, Taipei 10617, Taiwan ROC
[7] Research Center for Future Earth, National Taiwan University, Taipei 10617, Taiwan, ROC
[8] Institute of Global Environmental Change, Xi'an Jiatong University, Xi'an 710054, China
[9] Key Laboratory of Karst Dynamics, MLR, Institute of Karst Geology, CAGS, Guilin 541004, China
[10] Department of Earth and Environmental Sciences, University of Minnesota, Minneapolis, MN 55455, USA
[11] Department of Physics, Universitas Negeri Padang, Padang 25131, Indonesia

[*]Corresponding author: akimbrough@uow.edu.au

Abstract

Speleothem $\delta^{18}O$ is widely used as a proxy for rainfall amount in the tropics on glacial-interglacial to interannual scales. However, uncertainties in the interpretation of this renowned proxy pose a vexing problem in tropical paleoclimatology. Here, we present paired measurements of Mg/Ca and $\delta^{18}O$ for multiple stalagmites from southwest Sulawesi, Indonesia, that confirm changes in rainfall amount across ice age terminations. Collectively, the stalagmites span two glacial-interglacial transitions from 380 to 330 ky BP and 230 to 170 ky BP. Mg/Ca in our slow-growing stalagmites is affected by karst infiltration rates and prior calcite precipitation, making it a good proxy for changes in local rainfall. When paired, Mg/Ca and $\delta^{18}O$ corroborate prominent shifts from drier glacials to wetter interglacials in the core of the Australasian monsoon domain. Deviations between the two proxies may reveal concurrent changes in rainfall amount and moisture-transport pathways indicative of regional monsoon circulation.

Introduction

A basic understanding of the timing and magnitude of natural variability of tropical rainfall in the past is critical to place present trends in context and to validate climate model performance[1]. Much of modern society directly or indirectly relies on the consistency of seasonal rains for agriculture in tropical monsoon settings[2,3]. Reliable and well-constrained hydroclimate records from the tropics, and from the heavily populated Australasian monsoon domain in particular, are necessary for understanding processes driving monsoon strength and deep convection over the Indo-Pacific Warm Pool over multiple timescales. While ice cores, lake sediments, and tree-rings make up a large proportion of terrestrial paleoclimate records at the higher latitudes, speleothems provide exceptionally long, highly resolved and well-dated land-based archives of glacial-interglacial (G-I) rainfall variability at tropical latitudes[4–9]. At present, over 350 speleothem $\delta^{18}O$ records have been published for monsoon domains in Australasia and the Americas[10] (Fig. 1).

Early speleothem $\delta^{18}O$ records for the core area of the Australasian monsoon were interpreted in terms of the 'amount effect', and thus changes in the quantity of rainfall[11–14]. However, as the number of paleoclimate records for near-equatorial monsoonal settings grows, it has become clear that controls on speleothem $\delta^{18}O$ in these areas are complex and that interpreting this proxy simply in terms of local rainfall amount may not always be valid[15–20]. More recent works interpret $\delta^{18}O$ as a proxy that integrates the influence of regional convective activity, monsoon 'strength' and/or changes in moisture transport pathways[7,21,22]. Therefore, in tropical monsoon settings, the ideal situation would be to utilise a multi-proxy approach capable of separating the amount effect from

rainfall $\delta^{18}O$ influenced by source moisture and fractionation along transport pathways. A better understanding of the utility of speleothem $\delta^{18}O$, by far the most commonly used proxy for paleo-monsoon reconstructions, will improve our ability to identify the drivers of past monsoon rainfall variability. Glacial-interglacial transitions provide an opportunity to understand how globally-significant monsoon systems respond to periods of rapid warming. Information gained from tropical speleothem $\delta^{18}O$ combined with proxies sensitive to local rainfall can assist in attributing major changes in local rainfall amount to a particular shift in the regional hydrological system.

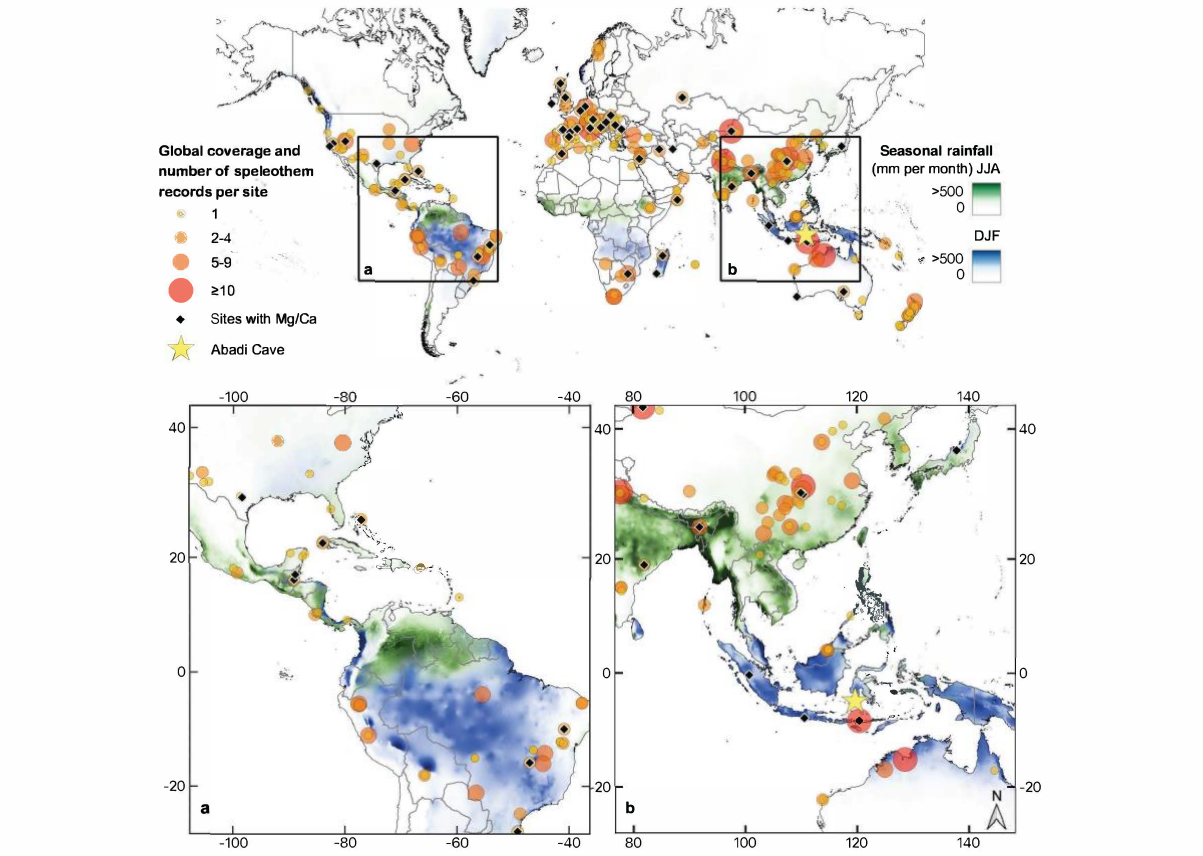

Fig. 1. Global distribution of speleothem $\delta^{18}O$ and Mg/Ca records and season-specific rainfall. Yellow star marks the location of the Sulawesi speleothem $\delta^{18}O$ and Mg/Ca records for this study. The global map is accompanied by insets: a) South American Monsoon region and b) Australasian Monsoon region. These areas were selected to illustrate speleothem $\delta^{18}O$ record density and Mg/Ca presence. Speleothem locations are from the SISAL V2 database[10]. The number of speleothem entities associated with each site is indicated by colour and size of circles. Black dots denote sites with Mg/Ca data reported in SISAL V2. Tropical rainfall for June-August (JJA, green scale) and December-February (blue scale), represents corresponding regional summer monsoon precipitation. Darker shades signify average monthly rainfall exceeding 500 mm. Precipitation data is from WorldClim 2.1 and span 1970-2000 at 5 minute resolution[73]. The map was created using QGIS software and country boundaries are based on the geometry from EBM v2020 (https://ec.europa.eu/eurostat/web/gisco/geodata/reference-data/administrative-units- statistical-units/countries).

Tandem measurements of speleothem Mg/Ca and $\delta^{18}O$ offer the possibility of decoupling local rainfall amount from variations in rainfall $\delta^{18}O$ due to changes in regional atmospheric circulation and source moisture[9,23–25]. Prior calcite precipitation (PCP) is recognized as a primary control on speleothem Mg/Ca variability and is controlled by effective infiltration (i.e., karst infiltration rate

and local rainfall amount)[26,27] and by the CO_2 content of cave air[28–30]. During periods of reduced rainfall, infiltration rate is reduced and water remains in the karst zone for extended periods. These conditions can cause increased void space in the karst and CO_2 degassing from seepage waters, which enhances the likelihood of calcite precipitating along flow pathways prior to the dripwater reaching a stalagmite surface[26,31]. The CO_2 content of air in the cave and void spaces drives the degassing process and is influenced by soil CO_2, atmospheric CO_2, and cave ventilation[30,32]. Time between drip intervals can also influence PCP[30]. Since calcite precipitation discriminates against both Mg and Sr in favour of Ca, PCP causes Mg/Ca and Sr/Ca in seepage waters upstream of the stalagmite to increase. Mg/Ca and Sr/Ca ultimately precipitated on the stalagmite will be elevated accordingly. Because of the preference for Ca to precipitate out of solution during PCP, coherency among measured stalagmite Mg/Sr[27] and the slope of the ln(Sr/Ca) and ln(Mg/Ca) regression line serve as a means to test for the occurrence of PCP[33,34]. It has also been shown that concentrations of Mg and Sr may be influenced by water-rock and water-soil contact times resulting in a covariation of Mg/Ca and Sr/Ca[30,32,35–37]. Because of the aforementioned processes, it is necessary to use multiple speleothems and a multi-proxy approach to produce accurate palaeohydrological records.

Few studies have reported on paired records of $\delta^{18}O$ and trace elements that span multiple G-I cycles[9,24,38]. Our study site in southwest Sulawesi, Indonesia, located in the core area of the Australasian monsoon with a strongly monsoonal climate, is ideally positioned to test the utility of speleothem $\delta^{18}O$ as a tropical rainfall indicator on G-I timescales (Fig. 1). Here, we use Mg/Ca (and Sr/Ca) in four southwest Sulawesi stalagmites spanning two G-I cycles to determine the suitability of $\delta^{18}O$ as a tropical rainfall indicator. We show that Sulawesi stalagmite Mg/Ca and Sr/Ca are primarily sourced from the limestone bedrock and subsequently altered by PCP. Variations in Mg/Ca and Sr/Ca of Sulawesi stalagmites with relatively slow growth are most likely driven by water-rock processes (i.e., PCP driven by infiltration, water residence time and void space availability), while fast-growing stalagmites appear to be more strongly influenced by soil-karst processes (i.e., PCP driven by the influenced of soil CO_2 on upper void spaces and conduits exposed to root respiration). The coherent pattern of variability between the slow-growing Mg/Ca and all four Sulawesi speleothem $\delta^{18}O$ records makes it possible to robustly interpret changes in local rainfall through major climatic transitions.

Our approach confirms a major increase in rainfall amount in the Australasian monsoon domain at glacial transitions that coincides with the largest shift in speleothem $\delta^{18}O$. Differences between Mg/Ca and $\delta^{18}O$ on sub-orbital timescales indicate an evolving balance between seasonal-scale

moisture-transport pathways or circulation, that don't necessarily reflect a corresponding change in rainfall amount. We therefore interpret the shift to more negative values in both proxies at the glacial termination as an increase in rainfall that was matched by a change in monsoon seasonality (more summer rainfall) and/or intensification of IPWP atmospheric circulation. These findings highlight the potential value of this multi-proxy approach for use elsewhere in the global monsoon system.

Study site and speleothem analysis

Stalagmites were collected from Abadi Cave in southwest Sulawesi, Indonesia (Lat. 5.0°S, Long. 119.7°E; elevation ~300 m above sea level). This region of southwest Sulawesi has highly seasonal rainfall, with the Indo-Australian summer monsoon delivering ~80% of annual rainfall between November and March. Mean annual temperature is 26.5°C. High-elevation topography to the southeast of the study site, including Mount Lompobatang (elevation 2,874 m), prevents much of the winter monsoon rainfall (June-August) from reaching the cave site[22,39].

Abadi Cave is approximately 320 m long and one of many systems carved within the Miocene Tonasa limestone formation that covers much of the southwestern region of Sulawesi[40]. The ground-surface above the cave is characterised by karst and lowland intermediate forest with thin soil profiles[41]. Abadi Cave has minor vertical changes of ±15 m and variable ceiling height. Although the cave's chambers are extensively decorated, active stalagmite growth has yet to be identified.

All stalagmite samples (Fig. 2) were collected approximately 250 m from the cave entrance. Stalagmites AC11-03 and AC11-02 grew in a large 'basement chamber' (~20 m across), while AC09-04 and AC11-06 were collected from a small 'side chamber' nearby and 10 above the 'basement chamber' (Fig. 2). Both chambers are isolated from the main entrance by a narrow crawl-through passageway. Stalagmite AC09-04 was found broken at the time of collection in 2009. The other three stalagmites were collected *in situ* in 2011 based on results from reconnaissance U-Th dating of mini-cores[39] drilled in 2009. Limestone bedrock material was collected near the entrance of Abadi Cave in 2011 (Supplementary Information).

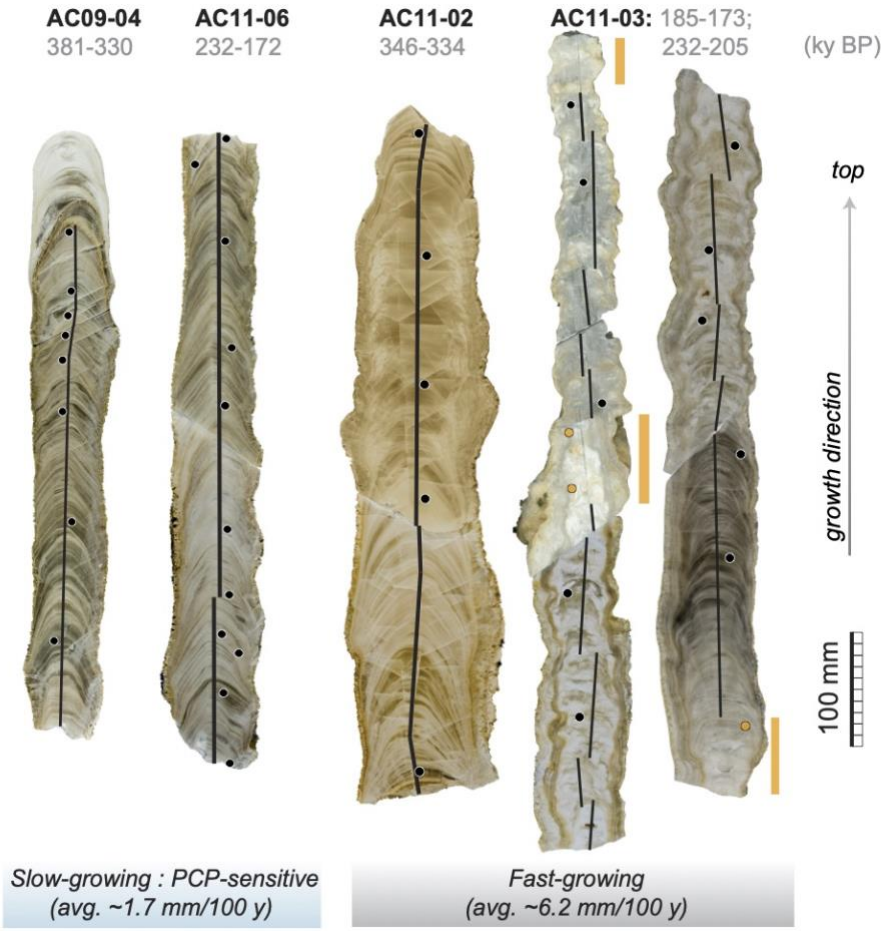

Fig. 2. Abadi Cave stalagmites analysed for this study. Photos of polished surfaces with sample milling tracks (black lines). U-Th date locations (black circles) are shown for each stalagmite. Note the uniform growth structure and clearly visible laminae on the slower-growing stalagmites, AC11-06 and AC09-04. The faster growing stalagmites, AC11-03 and AC11-02, tend to be broader and less uniform (varying diameter), with subtle and intermittent laminae. AC11-03 contains growth unconformities (yellow bars); these segments are excluded from the analysis. Three U-Th dates associated with these unconformities (yellow circles) are excluded from the final age-depth model.

Age models. The age-depth profiles of the Abadi Cave stalagmites are constrained by 34 high-precision U-Th dates (see Methods and Supplementary Table 1). Collectively, the geochemical records encompass ~100 ky of past climate, dating between 381 to 330 ky BP and 232 to 173 ky BP. Initial age-depth models for each stalagmite were constructed with the U-Th dates and a Bayesian age modelling approach using Bacon software and implemented in R[42,43] to produce weighted mean age-depth models with 95% confidence intervals for each stalagmite (see Methods and Supplementary Fig. 1-2).

The new stalagmite $\delta^{18}O$ timeseries for Sulawesi is well replicated, with common patterns clearly identified across sections of overlap (Fig. 3; and Supplementary Fig. 2). Therefore, the Bacon age models were optimized using linear interpolation between visual tie-points in the $\delta^{18}O$ records.

Sections of the Bacon age models were aligned by taking the average age of shared excursions and incorporating these sections into the original Bacon age-depth model. Importantly, all averaged tie-points and optimized age models fall within the age-depth uncertainties established using Bacon (Supplementary Fig. 2; Supplementary Tables 2 and 3). Because the individual stalagmite $\delta^{18}O$, Mg/Ca, and Sr/Ca records are each generated from the same sample aliquot, these age-depth models apply to each geochemical record described below. The age models show that growth rates for AC11-06 and AC09-04 (from the 'side chamber') are relatively slow (0.017 and 0.011 mm/y, respectively). In contrast, AC11-03 and AC11-02 (from the 'basement chamber') grew about four times faster (0.042 and 0.064 mm/y on average) with maximum growth occurring at glacial terminations.

Coupled analysis of $\delta^{18}O$, Mg/Ca and Sr/Ca. A total of 1,253 $\delta^{18}O$ and 683 paired Mg/Ca and Sr/Ca ratios were analyzed on aliquots of calcite powders micro-milled along the central growth axis of each stalagmite (see Methods). Mg/Ca and Sr/Ca were measured via inductively coupled plasma atomic emission spectroscopy on every second $\delta^{18}O$ sample for AC09-04 and AC11-06 and nearly every $\delta^{18}O$ sample for AC11-02 and AC11-03.

Measurements of Mg/Ca and Sr/Ca were made on a sample of surface bedrock limestone to determine the relationship between bedrock and stalagmite values (see Supplementary Information). Four spot-check analyses of Mg/Ca in the bedrock sample range from 12.1 to 13.2 mmol/mol, which is ~20 times higher than in the stalagmite samples. Bedrock Sr/Ca ranges from 0.24 to 0.28 mmol/mol, ~10 times higher than in the stalagmite samples. The large difference is due to the strong discrimination against Mg and Sr during the precipitation of stalagmite calcite from dripwaters with Mg/Ca and Sr/Ca compositions derived primarily from dissolved bedrock[31].

Results and Discussion

Geochemical and growth-rate profiles for the four Sulawesi stalagmites are presented in Figure 3. Stalagmite $\delta^{18}O$ values range between -10.2 and -4.9‰ after correction for the effect of ice volume[44,45] (Supplementary Information). The effect of temperature change on speleothem $\delta^{18}O$ at our site is deemed to be negligible[22] and the range of G-I change in $\delta^{18}O$ is much larger than can be explained by temperature[46]. The older stalagmites, AC09-04 and AC11-02 have $\delta^{18}O$ values that are consistently ~0.8‰ lower than the younger stalagmites, AC11-06 and AC11-03.

Mg/Ca and Sr/Ca for the younger stalagmites (AC11-06 and AC11-03) range from 0.25 to 1.0 mmol/mol and 0.009 to 0.025 mmol/mol, respectively. The older stalagmites (AC09-04 and AC11-02) have a slightly larger range of variability, with Mg/Ca values between 0.32 and 1.14 mmol/mol and Sr/Ca values between 0.013 and 0.044 mmol/mol. Due to the low concentrations of Sr in our samples, we focus on Mg/Ca for comparative analyses against $\delta^{18}O$.

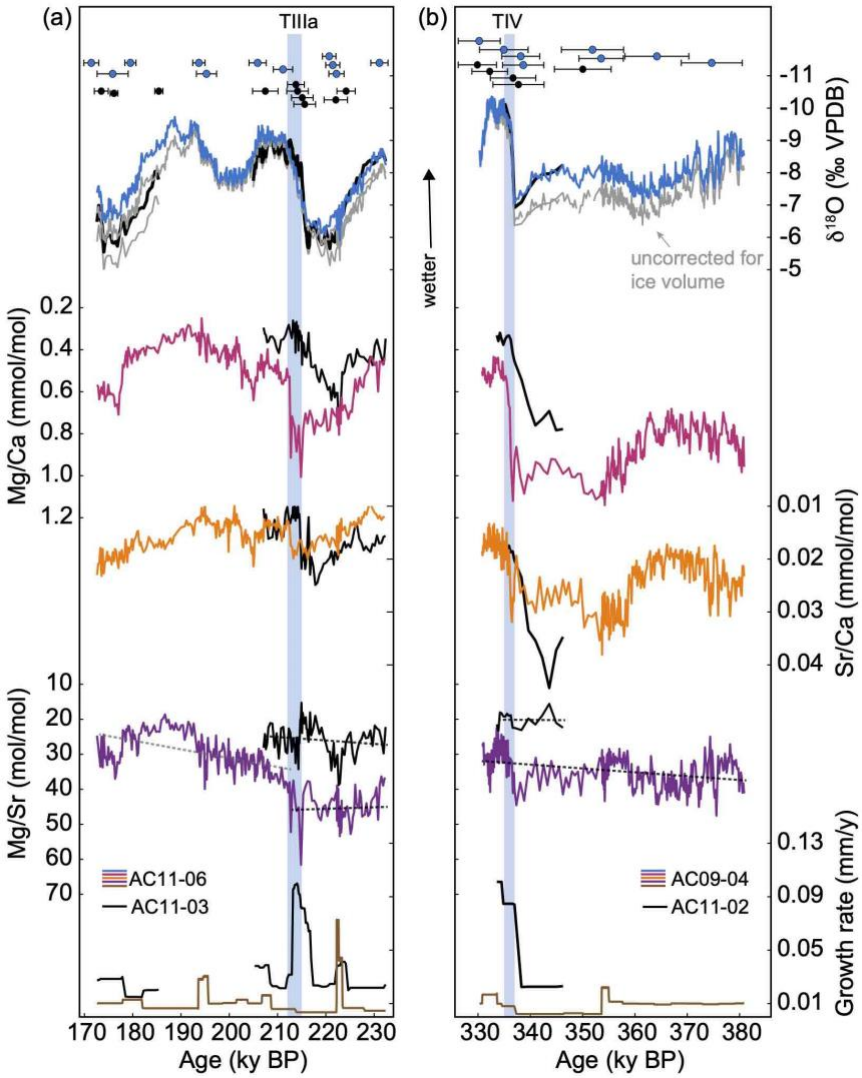

Fig. 3. Stalagmite $\delta^{18}O$, Mg/Ca, Sr/Ca and growth rates. (**a**) Stalagmites AC11-06 and AC11-03 for Termination IIIa and (**b**) AC09-04 and AC11-02 for Termination IV. Geochemical data for fast growing stalagmites (AC11-03, AC11-02) are shown in black, slow growing stalagmites (AC11-06, AC09-04) are colour coded. Stalagmite $\delta^{18}O$ has been corrected for the effect of ice volume; the uncorrected record is shown in grey (see Supplementary Material for details of this correction). Glacial terminations (determined by prominent shifts in Sulawesi stalagmite $\delta^{18}O$, Supplementary Information) are indicated by blue vertical bars. Colour-coded circles at the top of each panel show U-Th dates and their uncertainties (2□). Black dashed trendlines show where Mr/Sr is relatively constant, the grey dashed line shows trending Mg/Sr. The y-axes for geochemical profiles are inverted to show wetter conditions upward.

Karst recharge and PCP. Mg/Ca and Sr/Ca in speleothems are sensitive to the addition and removal of Ca from dripwaters through processes associated with soil and cave air CO_2 (soil-karst

interactions) and water-rock interactions/PCP along flow pathways[33,47,48]. If PCP occurs upstream of the cave drip site, the Mg/Ca and Sr/Ca will increase in the dripwater as Ca is preferentially lost from solution during PCP. Calcite precipitating from these waters on the speleothem surface will also be similarly co-enriched in Mg and Sr. PCP can occur when infiltration rates are low, drip intervals are long, or when cave CO_2 is low; these processes and combinations of processes can differ depending on the individual dripwater flow pathways feeding a stalagmite[30,35,37,49].

Stalagmite Mg/Sr is examined to assess whether Mg/Ca and Sr/Ca compositions have been altered by PCP (i.e by progressively losing Ca from solution)[27]. If PCP is the primary driver of Mg/Ca and Sr/Ca variability, then Mg/Sr should be constant through time. All Sulawesi stalagmite records show relatively constant Mg/Sr through time with the exception of the youngest section of AC11-06 (dating to 212-173 ky BP), trending towards lower values (Fig. 3). Wetter conditions during this interval could reduce PCP and increase the chance of mixing water reservoirs with different trace element compositions and sources (e.g., soil chemistry, re-routing of drip pathway, freshly weathered/broken bedrock). Thus, Mg/Ca is less effective as a hydroclimate indicator at times when the epikarst is in a fully saturated state[26,31,32]. Constant Mg/Sr throughout the Sulawesi records, and particularly over periods with higher elemental ratios, support the occurrence of PCP[27].

Sulawesi stalagmite Mg/Ca and Sr/Ca positively and significantly co-vary, further supporting the occurrence of PCP[27]. Using k-means cluster analysis, we identify two significant groupings of the Mg/Ca and Sr/Ca data for the Sulawesi stalagmites (Fig. 4). The Cluster 1 group has relatively low Mg/Ca and Sr/Ca values, supporting reduced PCP, while Cluster 2 has higher values, suggesting enhanced PCP. Notably, nearly all of the fast-growing stalagmite data and non-constant Mg/Sr data from AC11-06 are found in Cluster 1.

Speleothem Mg, Sr, and Ca are typically derived from the dissolved limestone bedrock and secondary minerals along flow pathways, but can also be sourced from the soil and atmosphere[26,32]. Notably, bedrock dissolution, and thus Mg, Sr, and Ca concentrations, can be influenced by soil CO_2 and groundwater infiltration rates[37].The measured Mg/Ca and Sr/Ca values for Abadi Cave bedrock and estimated partition coefficients[33,34,50,51] are used to calculate approximate Mg/Ca and Sr/Ca values for stalagmite calcite sourced entirely from the host rock, defined here as $bedrock_{sp}$ (see Supplementary Information; Supplementary Fig. 3). Calculated $bedrock_{sp}$ values plot alongside stalagmite Mg/Ca and Sr/Ca ratios associated with Cluster 1 (Fig. 4). Proximity of Cluster 1 data to the calculated $bedrock_{sp}$ implies limited evolution away from the original bedrock composition and

thus minimal PCP. Cluster 2 contains higher Mg/Ca and Sr/Ca values, which have evolved further away from the predicted bedrock$_{sp}$. This indicates increased PCP, potentially in response to groundwater recharge and rainfall amount at the surface of the cave.

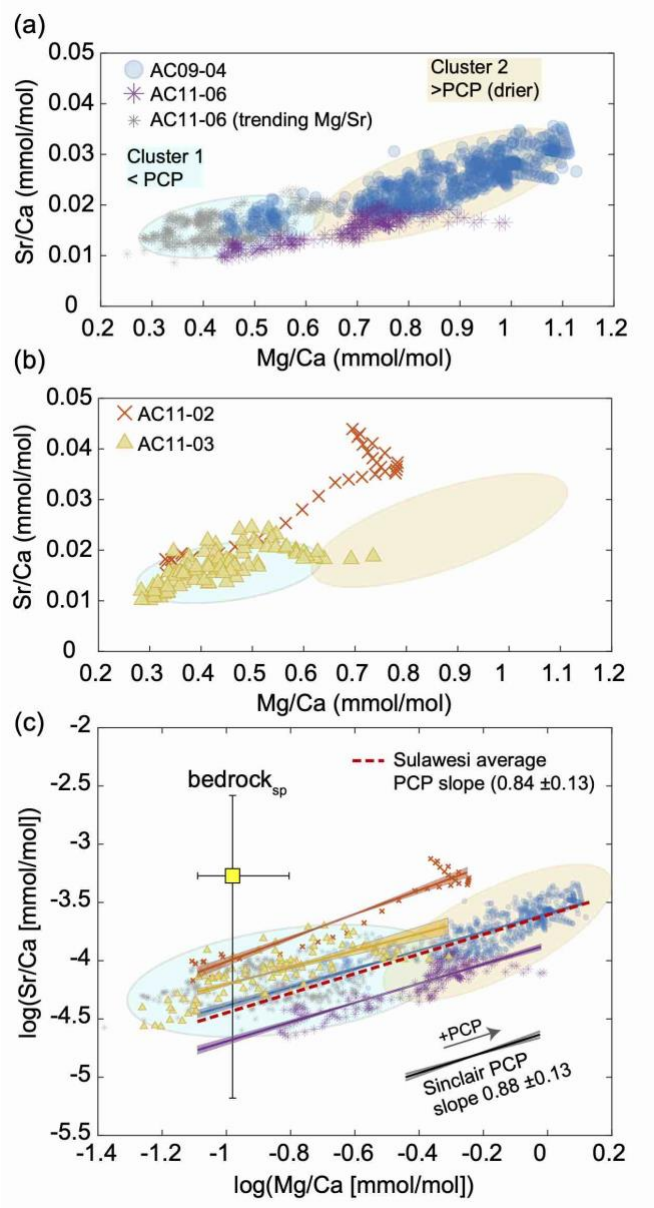

Fig. 4. Mg/Ca and Sr/Ca cluster analysis and log-log PCP test. Trace element ratios (mmol/mol) for **(a)** slow-growing stalagmites and **(b)** fast-growing stalagmites that have been resampled to evenly spaced intervals (Supplementary Table 5). **(c)** Comparison of ln(Mg/Ca) and ln(Sr/Ca) with regressions and bedrock$_{sp}$ alongside the theoretical PCP slope of Sinclair et al. (ref. 33). The Sulawesi average PCP slope is calculated using the average of each stalagmite regression. Slopes shown for individual records were calculated from resampled data. Regressions on original data (unevenly spaced) data made no significant difference in slopes (see Supplementary Figure 3 and Supplementary Table 5). The data-pairs in AC11-06 with trending Mg/Sr (grey asterisks) show limited PCP and are not included in the average Sulawesi PCP regression. k-means cluster analysis of Mg/Ca and Sr/Ca for all Sulawesi stalagmites: Cluster 1 (blue ellipse, 1.5s) grouping near average bedrock$_{sp}$ (yellow square with uncertainty range) is interpreted as minimal PCP while Cluster 2 (orange ellipse, 1.5s) has evolved away from bedrock$_{sp}$ towards higher values, indicating enhanced PCP. K-means cluster analysis (kmeans clustering), ellipse determination (ELLIPSATE) and linear regression (Linear Regression plot with Confidence Intervals) were performed and plotted in Matlab (https://au.mathworks.com/matlabcentral/fileexchange/).

The log-log relationship between Mg/Ca and Sr/Ca data can be used as an additional test for the occurrence of PCP where Mg/Sr is constant (Fig. 4). Previous work has shown that Mg/Ca and Sr/Ca increase predictably as PCP proceeds[27,31]. The relative increase of Mg and Sr in solution is driven by Mg-Ca and Sr-Ca partition coefficients that are both much less than one[26,52]. Sinclair et al. (ref. 33) developed a mathematical model of PCP showing that ln(Sr/Ca) versus ln(Mg/Ca) produces a positive vector of constant slope that falls within a range of 0.75 to 1.01. Mg/Ca and Sr/Ca regressions for each Sulawesi stalagmite record have a log-log slope within range of Sinclair's theoretical PCP slope (0.88 ±0.13) and well within the expanded range identified in Wassenburg et al (ref. 34). Each regression is slightly offset, indicating that the Mg and Sr content of individual stalagmites may be influenced by distinct dripwater flowpathways[37]. The average log-log slope of Sulawesi Mg/Ca and Sr/Ca data is 0.84 ±0.13. This average regression was calculated using resampled data (determined by the median resolution of each record) to obtain evenly spaced increments. The average regression slope for the raw data is also within the resampled PCP range (Supplementary Table 5).

Optimal stalagmites for recording hydrology-driven PCP. Both fast and slow-growing stalagmites show evidence for PCP; however, the slow-growing stalagmites demonstrate a clear trend away from $bedrock_{sp}$ towards more highly evolved Mg/Ca and Sr/Ca (spanning both Clusters 1 and 2). This suggests that PCP plays a larger role in their trace element chemistry than for fast growers. Moreover, when the Mg/Ca and Sr/Ca timeseries are considered for slow and fast-growing stalagmites that grew over the same time period, there are distinct differences in trends, implying that different processes are impacting site-specific flow pathways (Fig. 5). We note that the coeval stalagmite $\delta^{18}O$ records show excellent reproducibility and appear to be unaffected by differences in site-specific flow pathways. The slow-growing stalagmite Mg/Ca timeseries share the G-I baseline shift with stalagmite $\delta^{18}O$, transitioning to lighter values during glacial terminations. Conversely, Mg/Ca values in the faster growing stalagmites (Cluster 1) are more coherent with global atmospheric CO_2 fluctuations and global temperature[53–55], where lower Mg/Ca coincides with higher CO_2 and temperature (Fig. 5).

PCP is controlled by groundwater infiltration and the availability of air-filled voids within the karst aquifer (water-karst processes). PCP is also controlled by the CO_2 content of air in the cave and void spaces (soil-karst processes)[28,30,31]. Individual drip pathways and flow rates can determine which of these processes prevail for site specific drip waters[35,37,47]. Rainfall amount and infiltration through the karst influence the amount of void space where PCP can occur. Independent from changes in

rainfall, large G-I shifts in global temperature and CO_2 likely had a significant effect on soil and cave air CO_2 via vegetation and plant root respiration[56–58]. Total global emissions of CO_2 from soils is recognized as one of the largest fluxes in the global carbon cycle[59]. Modern studies show that elevated atmospheric CO_2 accelerates biogeochemical cycles and increases soil CO_2 [60,61]. In addition to driving changes in the CO_2 of voids, conduits, and cave air, a change in soil CO_2 and biological productivity can influence the amount of limestone dissolution and thus Mg/Ca and Sr/Ca concentrations in the dripwater. We propose that fracture and conduit flow pathways, sensitive to soil CO_2, are capable of driving outgassing and PCP of cave waters early in their transit to a stalagmite surface. Soil-karst PCP processes are likely to be imprinted in stalagmites that formed from dripwaters with a more direct path from soil-to-stalagmite, while water-rock processes are more likely to be imprinted in stalagmites fed by longer seepage dripwater flow pathways.

The slow-growing (~0.01-0.02 mm/y) Sulawesi stalagmites are uniformly narrow in diameter and likely fed by seepage flow, perhaps from soda straws, with relatively slow and regular drip intervals[47]. Dripwaters feeding the slow-growing stalagmites are hypothesised to travel through longer flow pathways, with increased water-rock interactions and extended exposure to void space, leading to enhanced PCP during periods of low infiltration. Thus, we propose that dripwaters feeding the slow-growing stalagmites were dominated by infiltration-driven PCP, where PCP increases with reduced rainfall and drives Mg/Ca towards higher values.

The fast-growing specimens (~0.04-0.06 mm/y), are characterised by relatively wide diameters that vary with height and are likely fed by variable drip rates, with a combination of fracture flow and diffuse flow[47]. Flow pathways for the fast-growing stalagmites may be subject to higher hydraulic loading, fewer air-filled voids and less water-rock interactions, resulting in a stronger chemical imprint from the soil and vadose zone. Given the faster growth rates and shared trends with atmospheric CO_2, we postulate that fast-growing stalagmites were predominantly imprinted by large (G-I) changes in soil CO_2 with infiltration-driven PCP operating as a secondary driver[26,30,47]. This novel working hypothesis would benefit from modern experiments in cave sites with active drips, accompanied by integrated modelling.

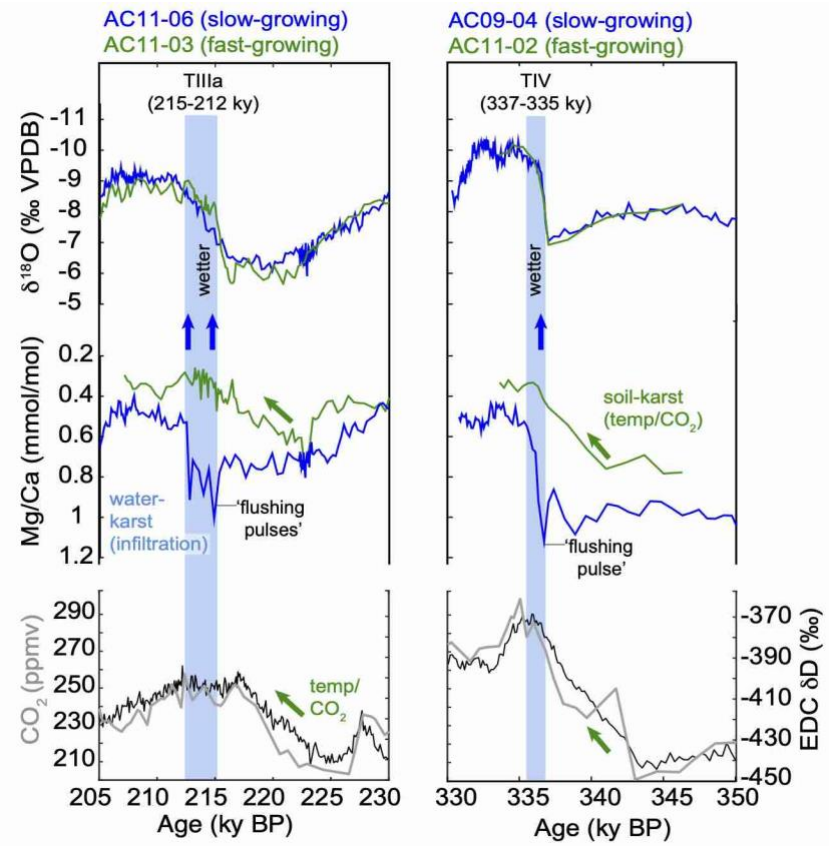

Fig. 5. Slow-growing vs. Fast-growing Sulawesi stalagmite $\delta^{18}O$ and Mg/Ca. Timeseries for Sulawesi stalagmite $\delta^{18}O$ and Mg/Ca (upper panels) and Vostok ice core measurements of atmospheric CO_2 (grey) and EPICA Dome C deuterium (black) plotted on the AICC chronology (bottom panel, Refs.[53–55]). The Sulawesi timeseries are color coded, with slow-growing stalagmites shown in blue and fast-growing stalagmites shown in green. The gradual trend in the fast-growing Mg/Ca (green) corresponds with changes in atmospheric CO_2 and global temperature/dD (green arrows). This Mg/Ca response is attributed to soil-karst processes, driven by vegetation changes. The step-change in the slow-growing stalagmite Mg/Ca (blue) corresponds with the $\delta^{18}O$ deglacial transition and is attributed to water-karst processes driven by infiltration. Note infiltration-related pulses during glacial terminations (see text for details). Black arrows show major transitions shared by $\delta^{18}O$ and slow-growing Mg/Ca. The duration of glacial terminations TIIIa (215–212 ky BP) and TIV (337–335 ky BP), are based on all four stalagmite $\delta^{18}O$ change points and coinciding change points in slow-growing stalagmite Mg/Ca (vertical blue bars, Supplementary Fig. 4).

Because PCP associated with the slow-growing Sulawesi stalagmites is more likely to be influenced by rainfall amount and effective recharge, Mg/Ca measurements from these stalagmites are better suited for hydrological reconstructions and comparison with $\delta^{18}O$. The exceptional length, reproducibility, and covariation of the slow-growing stalagmite records allows us to assess the validity of the heavily relied upon $\delta^{18}O$ rainfall proxy across G-I transitions. We therefore focus on the slow-growing stalagmites for comparison against $\delta^{18}O$.

Coupled Mg/Ca- $\delta^{18}O$ assessment of G-I transitions. The Mg/Ca values of the slow growing stalagmites (AC11-06 and AC09-04) share a prominent shift to lower values that coincides with the G-I transitions in $\delta^{18}O$. The good agreement between the paired proxies provides evidence for the preservation of a regional and locally-relevant climatic signal[62]. Additionally, the agreement between

all four Sulawesi $\delta^{18}O$ records and PCP-sensitive Mg/Ca of the slow-growing stalagmites indicates that both proxies are responding to rainfall amount at the glacial termination[26]. The onset of major G-I shifts in Sulawesi $\delta^{18}O$ and Mg/Ca are identified using Bayesian change-point analysis[63] (Supplementary Fig. 4). Stalagmite $\delta^{18}O$ undergoes a 3‰ shift to lower values over a 2-3 ky period, corresponding with glacial terminations IV (TIV: ~ 337–335 ky BP) and IIIa (TIIIa: ~215–212 ky BP). The Mg/Ca in the slow-growing stalagmites also undergoes a baseline shift to lower values during the $\delta^{18}O$ transition. The common trend of the two proxy datasets is consistent with drier glacial conditions with enhanced PCP, followed by increased rainfall and reduced/absent PCP during interglacials.

Using cross-correlation analysis, we show that the Mg/Ca glacial transition lags $\delta^{18}O$ by ~200 years for TIV (342–332 ky BP) and ~500-700 years for TIIIa (220–210 ky BP) – see Supplementary Fig. 5. Because the Mg/Ca and $\delta^{18}O$ measurements were made on the same sample aliquots, the lag cannot be due to chronological offsets between the two records. A slower re-saturation response of the karst network, i.e. filling voids and saturating diffuse flow pathways (indicated by Mg/Ca), relative to the more immediate response of seepage water reaching the stalagmite surface (indicated by $\delta^{18}O$) is the most likely explanation for such a delay[26,64]. For example, if a relatively dry karst network experiences a dramatic increase in groundwater availability due to increased rainfall, back-filling and saturation of the epikarst may take hundreds of years to measurably suppress the PCP system and dripwater Mg/Ca, whereas dripwater $\delta^{18}O$ would be influenced quickly by a change in the $\delta^{18}O$ of rainwater. When the karst network finally recovers from an extended glacial period of low-infiltration, the replenished water moving through the system is likely to entrain trace metals that have built up along flow-pathways during the dry periods and deposit them onto stalagmite surfaces[26]. Thus, the brief ‘pulse(s)’ towards higher Mg/Ca values, occurring over both terminations may signal the initial back-filling of the epikarst (Fig. 5).

There are subtle differences in the sub-orbital patterns of Mg/Ca and $\delta^{18}O$ from 375–355 ky BP when PCP is present (Fig. 6). The mismatch in the coupled record may indicate changes in the seasonal balance of rainfall, where changes in $\delta^{18}O$ are driven by changes in rainfall source and trajectories, rather than amount. Seasonal changes in the position of the ITCZ and Australasian monsoon moisture-transport pathways are accompanied by large latitudinal gradients in the $\delta^{18}O$ of rainfall[13,20]. The unexpectedly high rainfall $\delta^{18}O$ in Sulawesi around 375-355 ky BP corresponds to higher northern hemisphere summer insolation and monsoon rainfall in China[4]. A northward bias in the position of the ITCZ would decrease the contribution of austral summer rainfall and tip the

oxygen-isotope water balance in southwest Sulawesi toward isotopically heavier austral winter rainfall[13]. Additionally, variability in the Pacific Walker Circulation could influence regional rainfall $\delta^{18}O$ through changes in zonal moisture transport pathways and rainfall amount[65]. Therefore, unexpectedly high rainfall $\delta^{18}O$ in Sulawesi over this period could also be attributed to a weaker or displaced Pacific Walker Circulation that does not necessarily reflect changes in local rainfall amount[7,15].

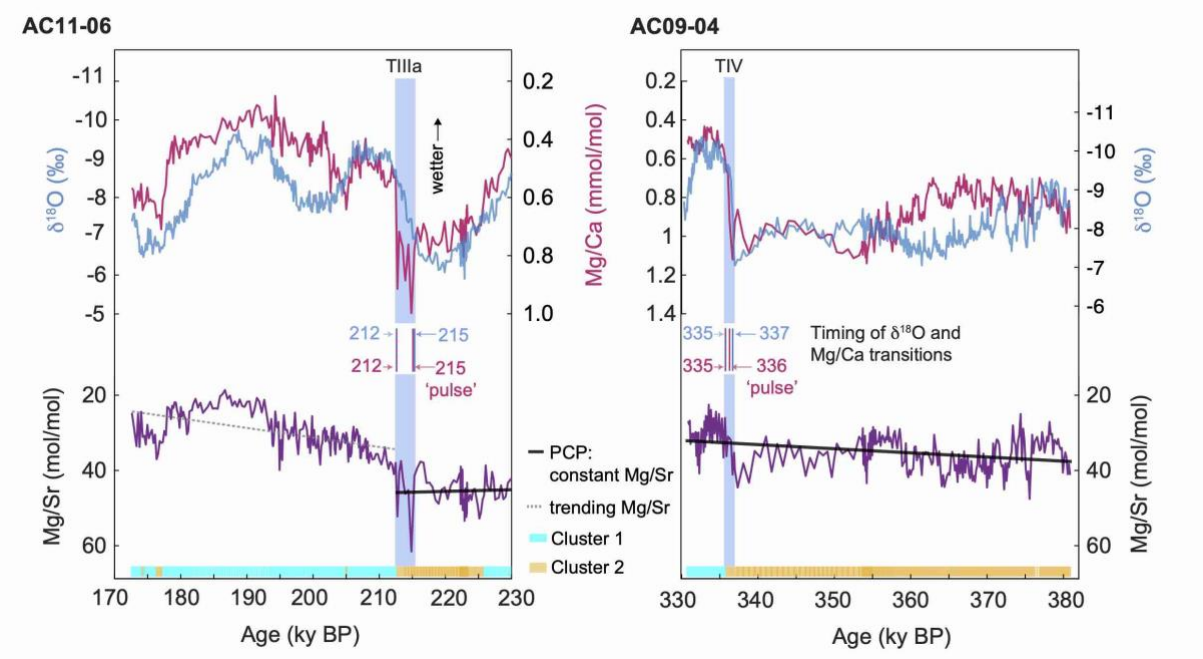

Fig. 6. Validation of the Sulawesi stalagmite Mg/Ca and $\delta^{18}O$ signals for terminations TIIIa and TIV. AC11-06 (left) and AC09-04 (right) stalagmite timeseries for $\delta^{18}O$ (blue), Mg/Ca (pink) and Mg/Sr (purple) with linear trends. Near-constant Mg/Sr values are indicated by black trend-lines, while trending Mg/Sr has a grey line. Cluster groupkings are shown for reference. Timing of G-I transitions in $\delta^{18}O$ (blue vertical bars) and Mg/Ca (pink vertical bars) was determined using change point analysis (Supplementary Fig. 4). Age annotations are in ky BP and 'pulse' refers to higher ratios occurring at termination onset (see main text). Blue vertical bars indicate the duration of glacial terminations TIIIa (215–212 ky BP) and TIV (337–335 ky BP).

Conclusions

The results presented here offer new insight into the potential for coupled records of stalagmite Mg/Ca and $\delta^{18}O$ to provide tighter constraints on interpretations of hydroclimate variation in the deep tropics where records of $\delta^{18}O$ alone can be ambiguous. A multi-proxy approach should be used when developing hydrological records from speleothems in these regions. A key finding from the coupled Mg/Ca and $\delta^{18}O$ records for Sulawesi is that glacial cycles in the core of the Australasian monsoon domain are characterised by a prominent and relatively rapid shift from dry glacials to wet interglacials at glacial terminations. Differences between Mg/Ca and $\delta^{18}O$ on sub-orbital timescales indicate that Sulawesi $\delta^{18}O$ may not always strictly record rainfall amount. Instead, rainfall $\delta^{18}O$

likely retains a combined signal of rainfall amount and the source or regional system from which that rain formed. With further development, discrepancies in coupled records of Mg/Ca and $\delta^{18}O$ for near-equatorial settings could become a powerful tool for distinguishing the relative contributions of summer and winter rainfall (with contrasting $\delta^{18}O$) to the monsoon water balance. When combined with other regional records, it may be possible to characterize major shifts in large atmospheric circulations systems, such as the Indo-Pacific Walker Circulation. An important goal for the paleoclimate community will be to establish criteria for identifying cave-sites containing speleothems with PCP signals driven by groundwater infiltration. Our results indicate that slow-growing and uniform stalagmites, located in sections of the cave with diffuse flow, are the most likely candidates to contain PCP-signals indicative of rainfall amount. An international effort to perform trace element analysis on existing high quality, well-dated, and relatively slow-growing stalagmites that have corresponding $\delta^{18}O$ measurements could provide a wealth of knowledge surrounding tropical climate dynamics.

Methods

Sample preparation. Following collection, stalagmites were cut in half and slabbed at ~15 mm thickness along the central plane of growth. Our method for sequential extraction of carbonate micro-samples from the specimens was adapted from existing techniques[32,66]. Briefly, calcite powders for stable isotopes ($\delta^{18}O$) and minor elements (Mg/Ca, Sr/Ca) were milled from the central growth axis of each stalagmite using a Sheridan GCM Micromill with a 1-mm-diameter end mill for high-resolution samples and a 2-mm-diameter end mill for low-resolution samples. High-resolution samples were milled continuously from stalagmites AC09-04 and AC11-06 at 0.8–1.2 mm increments, resulting in a sample resolution of 90–130 years and 40–180 years, respectively. The low-resolution samples presented in this work were milled at 10 and 30 mm increments, generating a sample resolution ranging between 80–740 years for AC11-03 and between 460–1890 years for AC11-02. High-resolution sampling was not performed on AC11-03 and AC11-02, as these samples were primarily intended for replication and high-resolution was not necessary. Four spot samples were milled for Mg/Ca and Sr/Ca analysis from clean, pre-milled surfaces of a single piece of surface bedrock material.

Uranium-thorium dating. Material for uranium-thorium (U-Th) dating was extracted from pre-cleaned surfaces of slabbed stalagmites using an impulse high torque air-drill fitted with a miniature circular saw blade. The saw blade was continuously lubricated with demineralized water while cutting. For each date, four cuts were made into the material allowing for the extraction the

extraction of a solid block weighing 130-200 mg. Numerous reconnaissance U-Th dates for this work were measured at the National Taiwan University's High-Precision Mass Spectrometry and Environment Change Laboratory (HISPEC). The majority of the 34 dates for the age-models used in this study were performed at the University of Minnesota Trace Metal Isotope Geochemistry Group (TMIG). The methodology for measuring U and Th isotopes by multi-collector inductively coupled plasma mass spectrometry (MC-ICP-MS) is described in Shen et al.[67,68] and Cheng et al.[69]. All U-Th isotope results and age determinations can be found in Supplementary Table S1. U-Th dates, relative to AD 1950, were corrected using the initial ^{230}Th value that minimized age reversals (Supplementary Fig. 1). Age errors (2s) on U-Th dates range from 0.5%-1.8%.

Age models. We used Bacon software[42], implemented through geoChronR[43], to construct initial age models for the stalagmite records in this study (Supplementary Figs. 1-2). Bacon is an age-depth modelling approach that uses Bayesian statistics to reconstruct accumulation histories based on U-Th dates and uncertainties. Millions of Markov Chain Monte Carlo (MCMC) iterations are used to estimate accumulation rates between depths, using information provided by U-Th dates and input parameters, such as estimated mean accumulation rates, memory, and sample thickness/slices. Bacon output consist of a weighted mean age-depth model with 95% confidence intervals. The Bacon age models were then optimized using linear interpolation between visual tie-points in the δ^{18}O records (Supplementary Tables 2-3, Supplementary Figs. 1-2). The tie-points and optimized age models for each stalagmite fall within the 95% confidence intervals of the original Bacon age-depth models.

Stable-isotope analysis. Measurements of stalagmite δ^{18}O were made at the Australian National University (ANU) using Finnigan MAT-251 and Thermo MAT-253 mass spectrometers, each coupled to a Kiel microcarbonate preparation device. To ensure consistency among runs, in-run measurements of the NBS-19 standard (δ^{18}O = -2.20‰) were made for every 5–8 samples, complemented by less frequent measurements of NBS-18 (δ^{18}O = -23.0‰). Results are reported relative to Vienna Peedee Belemnite (VPDB). The in-run analytical error for NBS-19, averaged for each run, is ±0.05‰ for δ^{18}O (n=375, 1σ). The mean standard error for duplicate analyses on sample aliquots was ±0.03‰ for δ^{18}O (n=64, 1σ). Quantifying instrumental errors and sample measurement reproducibility demonstrates that variability down to around 0.1‰ in the stalagmite δ^{18}O profiles is not due to measurement uncertainty. The powder samples for AC09-04 were alternately measured between instruments (i.e. odd numbered samples on the MAT-253, even numbered samples on the MAT-251). No significant offsets for δ^{18}O measurements were detected between the instruments for the purposes of this study.

Minor element measurements. Measurements of Mg/Ca and Sr/Ca in stalagmite and bedrock carbonate samples were measured on the same sample powders used for the stable isotope analyses using Varian Vista AX inductively coupled plasma atomic emission spectroscopy (ICP-AES) at the ANU. For the stalagmites milled at high resolution, every other sample was measured on the ICP-AES to preserve half of the sample material for future analyses. The ICP-AES analysis was based on methods described in Schrag (ref. 70) and de Villiers et al. (ref. 71) where a ~1 mg aliquot of carbonate powder was dissolved in 5 mL of 2% HNO_3. Each sample solution underwent 10 replicate analyses, with the final mmol/mol ratio reported as the average of all 10 replicate ratios. The internal precision of replicate measurements averaged over all runs is ±1.0% for Mg/Ca (mmol/mol) and ±1.7% for Sr/Ca (mmol/mol).

To standardize the ICP-AES data and account for potential instrument drift, standard-sample-standard bracketing was employed. ANU coral bracketing standards (Mg/Ca = 5.754 mmol/mol, Sr/Ca = 8.983 mmol/mol) were prepared from high purity $CaCO_3$, $SrCO_3$, and an AccuTrace 1000 ppm Mg standard, dissolved in 2% HNO_3. Bracketing standard trace element ratios were previously validated by thermal ionisation mass-spectrometry (TIMS) against an accepted ANU in-house standard. Bracketing standards had an average in-run precision of ±0.45% for Mg/Ca and ±0.29% for Sr/Ca (RSD, average of 64 analyses per run) over the course of 5–10 hour runs. Because the coral bracketing standard has higher concentrations of Sr than the Sulawesi stalagmite calcite, instrument rinse times between samples were increased to 180 seconds to avoid memory effects.

An additional synthetic standard with low Sr concentrations similar to those observed for southwest Sulawesi stalagmites (Sr/Ca = 0.02 mmol/mol), was used to test instrument detection limits. The precision for Sr/Ca ratios from the low Sr standard measurements was ±0.43% (n = 20, 1 RSD), thus demonstrating that the instrument is capable of precisely measuring low Sr concentrations. In-run measurements of the JCp-1 standard were also made to check the reproducibility among runs. Measurements for Mg/Ca and Sr/Ca ratios of JCp-1 (Mg/Ca = 4.125±0.028, Sr/Ca 8.766±0.032, n=11) are within error of those reported by Hathorne et al.[72] (Mg/Ca = 4.199±0.065, Sr/Ca 8.838±0.089), with a measurement precision of ±0.25% (n = 11, 1 RSD).

Data availability

Please email Alena Kimbrough for the data spreadsheets and tables mentioned in the manuscript and Supplementary Information.

References

1. Haywood, A. M. *et al.* What can Palaeoclimate Modelling do for you? *Earth Syst. Environ.* **3**, 1–18 (2019).
2. Muthayya, S., Sugimoto, J. D., Montgomery, S. & Maberly, G. F. An overview of global rice production, supply, trade, and consumption. *Ann. N. Y. Acad. Sci.* **1324**, 7–14 (2014).
3. Gaupp, F., Hall, J., Hochrainer-Stigler, S. & Dadson, S. Changing risks of simultaneous global breadbasket failure. *Nat. Clim. Chang.* **10**, 54–57 (2020).
4. Cheng, H. *et al.* Ice age terminations. *Science* **326**, 248–252 (2009).
5. Kathayat, G. *et al.* Indian monsoon variability on millennial-orbital timescales. *Sci. Rep.* **6**, 4–10 (2016).
6. Meckler, A. N., Clarkson, M. O., Cobb, K. M., Sodemann, H. & Adkins, J. F. Interglacial hydroclimate in the tropical west Pacific through the Late Pleistocene. *Science* **336**, 1301–1304 (2012).
7. Carolin, S. A. *et al.* Northern Borneo stalagmite records reveal West Pacific hydroclimate across MIS 5 and 6. *Earth Planet. Sci. Lett.* **439**, 182–193 (2016).
8. Denniston, R. F. *et al.* North Atlantic forcing of millennial-scale Indo-Australian monsoon dynamics during the Last Glacial period. *Quat. Sci. Rev.* **72**, 159–168 (2013).
9. Cruz Jr., F. W. *et al.* Evidence of rainfall variations in Southern Brazil from trace element ratios (Mg/Ca and Sr/Ca) in a Late Pleistocene stalagmite. *Geochim. Cosmochim. Acta* **71**, 2250–2263 (2007).
10. Comas-Bru, L. *et al.* SISALv2: A comprehensive speleothem isotope database with multiple age-depth models. *Earth Syst. Sci. Data Discuss.* 1–47 (2020) doi:10.5194/essd-2020-39.
11. Partin, J. W., Cobb, K. M., Adkins, J. F., Clark, B. & Fernandez, D. P. Millennial-scale trends in west Pacific warm pool hydrology since the Last Glacial Maximum. *Nature* **449**, 452–455 (2007).
12. Lewis, S. C. *et al.* High-resolution stalagmite reconstructions of Australian–Indonesian monsoon rainfall variability during Heinrich stadial 3 and Greenland interstadial 4. *Earth Planet. Sci. Lett.* **303**, 133–142 (2011).
13. Griffiths, M. L. *et al.* Increasing Australian–Indonesian monsoon rainfall linked to early Holocene sea-level rise. *Nat. Geosci.* **2**, 636–639 (2009).
14. Carolin, S. A. *et al.* Varied response of western Pacific hydrology to climate forcings over the last glacial period. *Science* **340**, 1564–1566 (2013).
15. Moerman, J. W. *et al.* Diurnal to interannual rainfall $\delta^{18}O$ variations in northern Borneo driven by regional hydrology. *Earth Planet. Sci. Lett.* **369**–**370**, 108–119 (2013).
16. Caley, T., Roche, D. M. & Renssen, H. Orbital Asian summer monsoon dynamics revealed using an isotope-enabled global climate model. *Nat. Commun.* **5**, 1–6 (2014).
17. Konecky, B., Russell, J. & Bijaksana, S. Glacial aridity in central Indonesia coeval with intensified monsoon circulation. *Earth Planet. Sci. Lett.* **437**, 15–24 (2016).
18. Liu, G. *et al.* On the glacial-interglacial variability of the Asian monsoon in speleothem $\delta^{18}O$ records. *Sci. Adv.* **6**, 1–11 (2020).
19. Nilsson-Kerr, K., Anand, P., Holden, P. B., Clemens, S. C. & Leng, M. J. Dipole patterns in tropical precipitation were pervasive across landmasses throughout Marine Isotope Stage 5. *Commun. Earth Environ.* **2**, 1–9 (2021).
20. Cobb, K. M., Adkins, J. F., Partin, J. W. & Clark, B. Regional-scale climate influences on temporal variations of rainwater and cave dripwater oxygen isotopes in northern Borneo. *Earth Planet. Sci. Lett.* **263**, 207–220 (2007).
21. Ayliffe, L. K. *et al.* Rapid interhemispheric climate links via the Australasian monsoon during the last deglaciation. *Nat. Commun.* **4**, 1–6 (2013).
22. Krause, C. E. *et al.* Spatio-temporal evolution of Australasian monsoon hydroclimate over the last 40,000 years. *Earth Planet. Sci. Lett.* **513**, 103–112 (2019).
23. Griffiths, M. L. *et al.* Western Pacific hydroclimate linked to global climate variability over the past two millennia. *Nat. Commun.* **7**, 1–9 (2016).
24. Magiera, M. *et al.* Local and regional Indian Summer Monsoon precipitation dynamics during Termination II and the Last Interglacial. *Geophys. Res. Lett.* **46**, 12454–12463 (2019).
25. Liu, Y. H. *et al.* Links between the East Asian monsoon and North Atlantic climate during the 8,200 year event. *Nat. Geosci.* **6**, 117–120 (2013).
26. Fairchild, I. J. & Treble, P. C. Trace elements in speleothems as recorders of environmental change. *Quat. Sci. Rev.* **28**, 449–468 (2009).
27. Tremaine, D. M. & Froelich, P. N. Speleothem trace element signatures: A hydrologic geochemical study of modern cave dripwaters and farmed calcite. *Geochim. Cosmochim. Acta* **121**, 522–545 (2013).
28. Spötl, C., Fairchild, I. J. & Tooth, A. F. Cave air control on dripwater geochemistry, Obir Caves (Austria): Implications for speleothem deposition in dynamically ventilated caves. *Geochim. Cosmochim. Acta* **69**, 2451–2468 (2005).
29. Baker, A., Flemons, I., Andersen, M. S., Coleborn, K. & Treble, P. C. What determines the calcium

concentration of speleothem-forming drip waters? *Glob. Planet. Change* **143**, 152–161 (2016).
30. Stoll, H. M., Müller, W. & Prieto, M. I-STAL, a model for interpretation of Mg/Ca, Sr/Ca and Ba/Ca variations in speleothems and its forward and inverse application on seasonal to millennial scales. *Geochem. Geophys. Geosyst.* **13**, 1–27 (2012).
31. Fairchild, I. J. *et al.* Controls on trace element (Sr–Mg) compositions of carbonate cave waters: implications for speleothem climatic records. *Chem. Geol.* **166**, 255–269 (2000).
32. Fairchild, I. J. *et al.* Modification and preservation of environmental signals in speleothems. *Earth-Science Rev.* **75**, 105–153 (2006).
33. Sinclair, D. J. *et al.* Magnesium and strontium systematics in tropical speleothems from the Western Pacific. *Chem. Geol.* **294**, 1–17 (2012).
34. Wassenburg, J. A. *et al.* Calcite Mg and Sr partition coefficients in cave environments: Implications for interpreting prior calcite precipitation in speleothems. *Geochim. Cosmochim. Acta* **269**, 581–596 (2020).
35. McDonald, J., Drysdale, R., Hill, D., Chisari, R. & Wong, H. The hydrochemical response of cave drip waters to sub-annual and inter-annual climate variability, Wombeyan Caves, SE Australia. *Chem. Geol.* **244**, 605–623 (2007).
36. Wong, C. I., Banner, J. L. & Musgrove, M. L. Seasonal dripwater Mg/Ca and Sr/Ca variations driven by cave ventilation: Implications for and modeling of speleothem paleoclimate records. *Geochim. Cosmochim. Acta* **75**, 3514–3529 (2011).
37. Oster, J. L., Covey, A. K., Lawrence, C. R., Giannetta, M. G. & Druhan, J. L. A reactive transport approach to modeling cave seepage water chemistry II: Elemental signatures. *Geochim. Cosmochim. Acta* **311**, 353–373 (2021).
38. Cheng, H. *et al.* Climate variations of Central Asia on orbital to millennial timescales. *Sci. Rep.* **5**, 1–11 (2016).
39. Scroxton, N. *et al.* Natural attrition and growth frequency variations of stalagmites in southwest Sulawesi over the past 530,000 years. *Palaeogeogr. Palaeoclimatol. Palaeoecol.* **441**, 823–833 (2015).
40. Wilson, M. E. J. & Bosence, D. W. J. The Tertiary evolution of South Sulawesi: a record in redeposited carbonates of the Tonasa Limestone Formation. *Geol. Soc. London, Spec. Publ.* **106**, 365–389 (1996).
41. Cannon, C. H., Harting, J., Salim, A. & Summers, M. *The vegetation of Sulawesi: Coarse filter analysis*. *Technical Report, The Nature Conservancy & Texas Tech University* (2005).
42. Blaauw, M. & Christen, J. A. Flexible paleoclimate age-depth models using an autoregressive gamma process. *Bayesian Anal.* **6**, 457–474 (2011).
43. McKay, N. P., Emile-Geay, J. & Khider, D. geoChronR – an R package to model, analyze, and visualize age-uncertain data. *Geochronology* **3**, 149–169 (2021).
44. Schrag, D. P., Hampt, G. & Murray, D. W. Pore fluid constraints on the temperature and oxygen isotopic composition of the glacial ocean. *Science* **272**, 1930–1932 (1996).
45. Bintanja, R., van de Wal, R. S. W. & Oerlemans, J. Modelled atmospheric temperatures and global sea levels over the past million years. *Nature* **437**, 125–128 (2005).
46. Yuan, D. *et al.* Timing, duration, and transitions of the last interglacial Asian monsoon. *Science* **304**, 575–578 (2004).
47. Baldini, J. U. L., McDermott, F. & Fairchild, I. J. Spatial variability in cave drip water hydrochemistry: Implications for stalagmite paleoclimate records. *Chem. Geol.* **235**, 390–404 (2006).
48. Sinclair, D. J. Two mathematical models of Mg and Sr partitioning into solution during incongruent calcite dissolution. *Chem. Geol.* **283**, 119–133 (2011).
49. Belli, R. *et al.* Investigating the hydrological significance of stalagmite geochemistry (Mg, Sr) using Sr isotope and particulate element records across the Late Glacial-to-Holocene transition. *Geochim. Cosmochim. Acta* **199**, 247–263 (2017).
50. Fairchild, I. J. & Baker, A. *Speleothem Science: From Process to Past Environments*. (Wiley-Blackwell, 2012).
51. Lorens, R. B. Sr, Cd, Mn and Co distribution coefficients in calcite as a function of calcite precipitation rate. *Geochim. Cosmochim. Acta* **45**, 553–561 (1981).
52. Holland, H. D., Kirsipu, T. V, Huebner, J. S. & Oxburgh, U. M. On some aspects of the chemical evolution of cave waters. *J. Geol.* **72**, 36–67 (1964).
53. Petit, J. R. *et al.* Climate and atmospheric history of the past 420,000 years from the Vostok ice core, Antarctica. *Nature* **399**, 429–436 (1999).
54. Bazin, L. *et al.* An optimized multi-proxy, multi-site Antarctic ice and gas orbital chronology (AICC2012): 120-800 ka. *Clim. Past* **9**, 1715–1731 (2013).
55. Jouzel, J. *et al.* Orbital and millennial Antarctic climate variability over the past 800,000 years. *Science* **317**, 793–796 (2007).
56. Breecker, D. O. *et al.* The sources and sinks of CO2 in caves under mixed woodland and grassland vegetation. *Geochim. Cosmochim. Acta* **96**, 230–246 (2012).
57. Breecker, D. O. Atmospheric pCO2 control on speleothem stable carbon isotope compositions. *Earth Planet. Sci. Lett.* **458**, 58–68 (2017).

58. Fohlmeister, J. *et al.* Main controls on the stable carbon isotope composition of speleothems. *Geochim. Cosmochim. Acta* **279**, 67–87 (2020).
59. Schlesinger, W. H. & Andrews, J. A. Soil respiration and the global carbon cycle. *Biogeochemistry* **48**, 7–20 (2000).
60. Lagomarsino, A., Lukac, M., Godbold, D. L., Marinari, S. & De Angelis, P. Drivers of increased soil respiration in a poplar coppice exposed to elevated CO_2. *Plant Soil* **362**, 93–106 (2013).
61. Kuzyakov, Y., Horwath, W. R., Dorodnikov, M. & Blagodatskaya, E. Review and synthesis of the effects of elevated atmospheric CO_2 on soil processes: No changes in pools, but increased fluxes and accelerated cycles. *Soil Biol. Biochem.* **128**, 66–78 (2019).
62. Dorale, J. A. & Liu, Z. Limitations of Hendy test criteria in judging the paleoclimatic suitability of speleothems and the need for replication. *J. Cave Karst Stud.* **71**, 73–80 (2009).
63. Ruggieri, E. A Bayesian approach to detecting change points in climatic records. *Int. J. Climatol.* **33**, 520–528 (2012).
64. Hellstrom, J. C. & McCulloch, M. T. Multi-proxy constraints on the climatic significance of trace element records from a New Zealand speleothem. *Earth Planet. Sci. Lett.* **179**, 287–297 (2000).
65. Falster, G., Konecky, B., Madhavan, M., Stevenson, S. & Coats, S. Imprint of the Pacific Walker Circulation in Global Precipitation $\delta^{18}O$. *J. Clim.* **34**, 8579–8597 (2021).
66. Gagan, M. K., Chivas, A. R. & Isdale, P. J. High-resolution isotopic records from corals using ocean temperature and mass-spawning chronometers. *Earth Planet. Sci. Lett.* **121**, 549–558 (1994).
67. Shen, C.-C. *et al.* Uranium and thorium isotopic and concentration measurements by magnetic sector inductively coupled plasma mass spectrometry. *Chem. Geol.* **185**, 165–178 (2002).
68. Shen, C.-C. *et al.* High-precision and high-resolution carbonate ^{230}Th dating by MC-ICP-MS with SEM protocols. *Geochim. Cosmochim. Acta* **99**, 71–86 (2012).
69. Cheng, H. *et al.* Improvements in ^{230}Th dating, ^{230}Th and ^{234}U half-life values, and U–Th isotopic measurements by multi-collector inductively coupled plasma mass spectrometry. *Earth Planet. Sci. Lett.* **371**–**372**, 82–91 (2013).
70. Schrag, D. P. Rapid analysis of high-precision Sr/Ca ratios in corals and other marine carbonates. *Paleoceanography* **14**, 97–102 (1999).
71. de Villiers, S., Greaves, M. & Elderfield, H. An intensity ratio calibration method for the accurate determination of Mg/Ca and Sr/Ca of marine carbonates by ICP-AES. *Geochem. Geophys. Geosyst.* **3**, 1–14 (2002).
72. Hathorne, E. C. *et al.* Interlaboratory study for coral Sr/Ca and other element/Ca ratio measurements. *Geochem. Geophys. Geosyst.* **14**, 3730–3750 (2013).
73. Fick, S. E. & Hijmans, R. J. WorldClim 2: new 1-km spatial resolution climate surfaces for global land areas. *Int. J. Climatol.* **37**, 4302–4315 (2017).

Acknowledgements

The project was carried out in Indonesia under Kementerian Negara Riset dan Teknologi (RISTEK) research permit numbers 04/TKPIPA/FRP/SM/IV/2009, 1b/TKPIPA/FRP/SM/I/2011 and 1889/TKPIPA/FRP/SM/V/2013. We thank the Research Center for Geotechnology, Indonesian Institute of Sciences (LIPI) for logistical support and are indebted to Baharudin (of Konservasi Sumber Daya Alam) and the staff of Bantimurung-Bulusaraung National Park (with special thanks to Syaiful Fajrin). Engkos Kosasih, Djupriono, Neil Anderson, Dan Zwartz, Garry Smith, Linda Ayliffe, Nick Scroxton, Joel Zwartz and Daniel Becker provided invaluable technical assistance in the field. We also thank Linda McMorrow, Joan Cowley, Heather Scott-Gagan, Joe Cali, Katharine Grant, Daniel Becker, and Hailong Sun for laboratory assistance. This study was supported by Australian Research Council *Discovery* Project grants DP0663274, DP1095673, DP110101161, and DP180103762 to M.K.G., W.S.H., R.L.E, H.C. and C-C.S.; an Australian Postgraduate Award and International Postgraduate Research Scholarship to A.K.K.; Science Vanguard Research Program of

the Ministry of Science and Technology (110-2123-M-002-009), the Higher Education Sprout Project of the Ministry of Education, Taiwan, ROC (110L901001), and National Taiwan University (110L8907) to C.-C.S.; U.S. National Science Foundation grants (1103402) and (1702816) to R.L.E. and H.C.; and National Natural Science Foundation of China grants to H.C. (NSFC 41731174 and NSFC 41888101).

Author contributions

M.K.G. conceived the project; A.K.K. and M.K.G. designed the project; B.W.S., G.B.D., M.K.G., H.R., A.K.K. and W.S.H. performed the fieldwork; C-C.S., H.-M.H., H.C. and R.L.E. carried out the reconnaissance and sample U-Th dating, with C-C.S. and H.-M.H. carrying out a significant portion of the reconnaissance dating for effective stalagmite selection; A.K.K. carried out the laboratory work and data analysis. A.K.K wrote the manuscript with draft reviews from M.K.G and input from all co-authors.

Competing interests

The authors declare no competing interests.

Supplementary Information

Supplementary Figures

Supplementary Data 1 (xlsx file upon request)

Initial $^{230}Th/^{232}Th$ correction on U-Th dates

Initial $^{230}Th/^{232}Th$ corrections are applied to the Sulawesi stalagmite U-Th age determinations to account for varying degrees of non-radiogenic detrital ^{230}Th contamination incorporated into the stalagmite during deposition. Detrital ^{230}Th contamination results in U-Th dates appearing too old. Detrital and hydrogenous materials are the most likely sources of initial ^{230}Th in speleothems[1]. Because ^{232}Th is non-soluble and accompanies detrital ^{230}Th, measured $^{230}Th/^{232}Th$ can give some indication of the amount of ^{230}Th contamination present in a dated sample, with lower ratios indicating higher levels of contamination[2,3]. Samples with higher levels of detrital ^{230}Th will have incorrect ages and be more significantly influenced by an initial Th correction. The average crustal $^{230}Th/^{232}Th$ activity ratio of 0.8 ±0.4 (atomic ratio $4.4 \pm 2.2 \times 10^{-6}$) is often used to correct speleothem U-Th dates; this ratio, however, varies substantially depending on the source material (e.g., overlying soil composition and local bedrock)[2,3]. Detrital ^{230}Th mainly is delivered to a stalagmite attached to detritus in dripwater and different flow pathways can introduce additional variability in detrital ^{230}Th that reaches the stalagmite. Additionally, as soil compositions and flow-

pathways evolve over time, and under different climate regimes, detrital $^{230}Th/^{232}Th$ can vary greatly within a single cave system[4,5].

For this work, we determined a suitable correction by testing a series of initial $^{230}Th/^{232}Th$ values to identify which value brought the stratigraphic sequence of age determinations for each stalagmite into maximal alignment (i.e., minimized age-reversals) (Supplementary Fig. 1). The initial $^{230}Th/^{232}Th$ activity values used on Sulawesi stalagmites are 3±1.5 (atomic ratio $16 \pm 8 \times 10^{-6}$) for AC11-06, AC11-03 and AC11-02 and 14±7 (atomic ratio $75 \pm 37.5 \times 10^{-6}$) for AC09-04. The errors on the initial activity ratios are arbitrarily set at 50%. We note that a larger initial correction on AC09-04 (e.g., 30-35 initial $^{230}Th/^{232}Th$ activity) would further improve alignment of the three dates (between 339 and 334 ky BP), but these three dates remain within error of each other regardless of the correction. We hesitate to apply such a large correction (10 times that of the other stalagmites) until there is additional evidence, such as additional replicate records or isochrons, to support it. Initial Th corrections were applied to the equation for U-Th age determination[2,6] using a Monte-Carlo approach to simulate >10,000 possible solutions within error of the measured geochemical variables. This approach accurately reproduces uncorrected dates provided by the dating facilities and generates 2s uncertainties on the corrected ages. Corrected U-Th dates (Table S1) were used to inform the Bacon age models[7,8] and tie-point optimized age models (Supplementary Fig. 2).

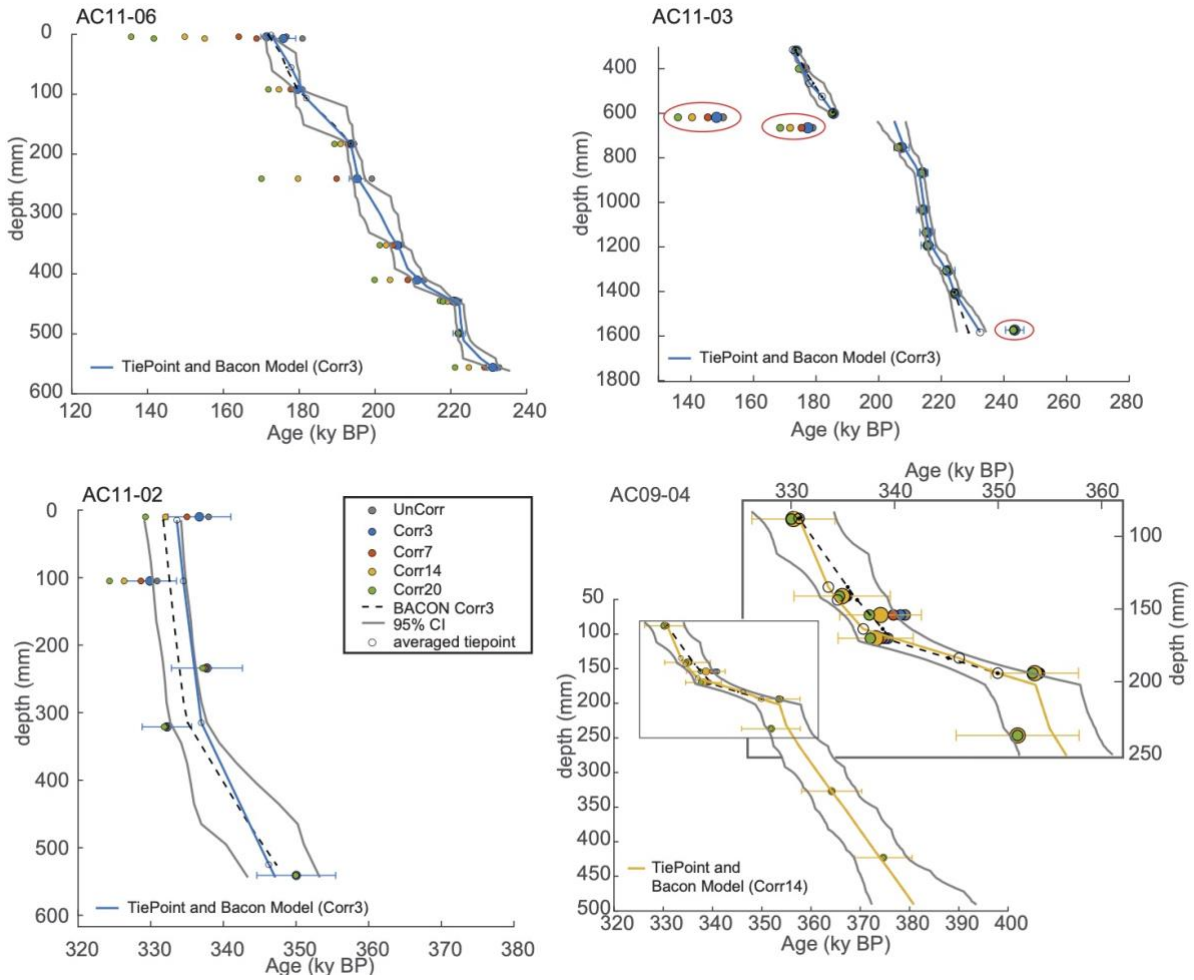

Supplementary Figure 1. Stalagmite age-depth models with initial $^{230}Th/^{232}Th$ corrections on U-Th dates. The process for determining the initial $^{230}Th/^{232}Th$ correction for each Sulawesi stalagmite (AC09-04, AC11-02, AC11-03, AC11-06). Final correction values were chosen based on minimization of age reversals for improved stratigraphic alignment. Tested initial $^{230}Th/^{232}Th$ activity ratios include: 0 or uncorrected (grey), 3±1.5 (blue), 7±3.5 (red), 14±7 (yellow) and 20±10 (green). The best-fit initial corrections are 3±1.5 (blue) for AC11-06, AC11-03 and AC11-02 and 14±7 (yellow) for AC09-04. The resulting corrected U-Th dates and 2s error bars are indicated by color. Bacon age models are constructed using the corrected U-Th dates. Final age-depth models utilising Bacon and tie-points are discussed in the main text. Three dates were excluded from the AC11-03 age-depth modes (circled in red) due to unconformities and unresolvable age reversals.

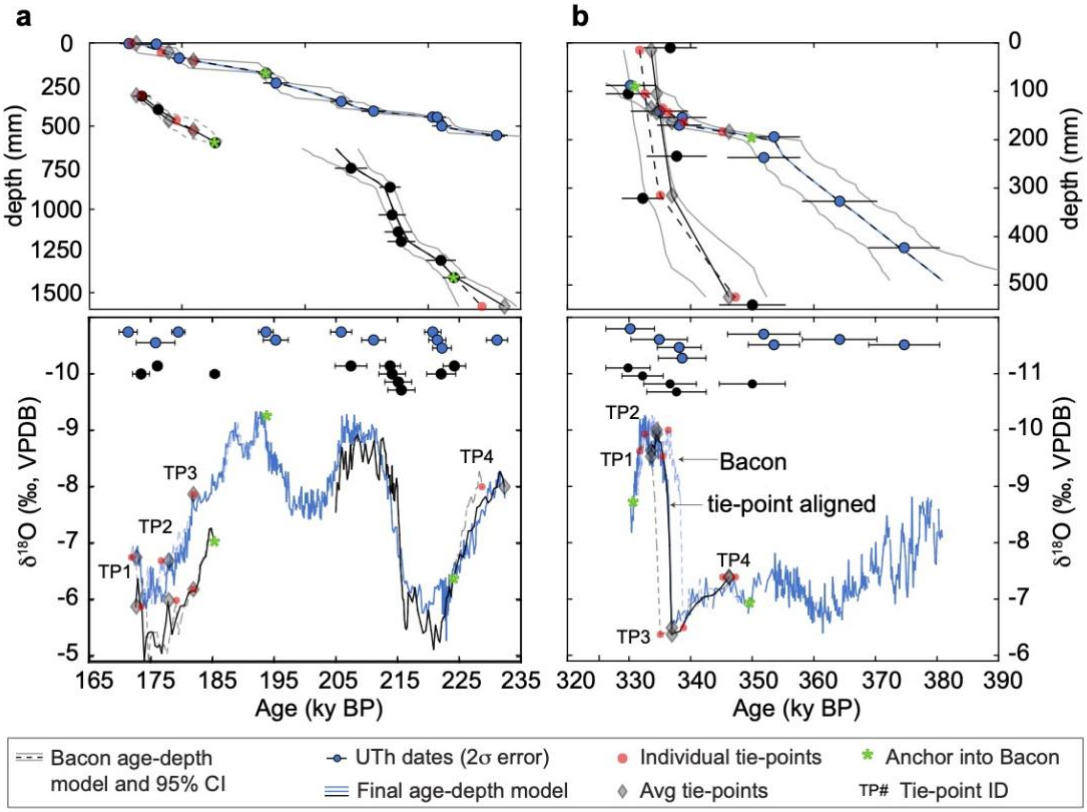

Supplementary Figure 2. Sulawesi stalgmite age-depth models with tie-point aligned $\delta^{18}O$ profiles. Age-depth models and stalagmite $\delta^{18}O$ timeseries are plotted for (**a**) TIII stalagmites AC11-06 (blue) and AC11-03 (black) and (**b**) TIV stalagmites AC09-04 (blue) and AC11-02 (black). Tie points are used to better align common features of the Sulawesi records within the 95% confidence intervals of Bacon age-depth models (dashed lines) to generate tie-point adjusted age models (solid lines). Age-depth models are shown in the upper panels and $\delta^{18}O$ timeseries (not corrected for ice volume) are shown in the lower panels. Colour-coded circles show U-Th dates (with 2σ errors) for each record. The timing of related $\delta^{18}O$ tie points (red dots) are averaged (diamonds) and merged into each stalagmite's Bacon age-depth model using linear interpolation between successive anchor points (green asterisks). Depth is relative to the top of the stalagmite. For further details see Supplementary Tables S2 and S3.

Ice volume correction

Stalagmite $\delta^{18}O$ values have been corrected for the effect of ice volume using a modelled ice sheet contribution to the marine oxygen-isotope signal[9], where a 120 m sea-level-rise equates to a -1‰ change in the $\delta^{18}O$ of seawater[9,10]. The ice volume correction was interpolated onto each stalagmite age-scale and subtracted from the corresponding measured stalagmite $\delta^{18}O$ value. Corrected and uncorrected stalagmite $\delta^{18}O$ values are shown in grey in main text Figure 3. Only the corrected $\delta^{18}O$ values have been used for climatic interpretation.

Sulawesi bedrock

A single piece of bedrock was collected near the entrance of Abadi Cave in 2011. Four spot samples were milled from the bedrock sample for Mg/Ca and Sr/Ca analysis. The bedrock measurements and calculation of $bedrock_{sp}$ (speleothem calcite forming from dripwaters with unaltered compositions)

are not critical for determining the occurrence of PCP, but they do provide a useful reference point for stalagmite Mg/Ca and Sr/Ca values expected from bedrock prior to the onset of PCP. The observation that the Sulawesi PCP line-of-fit intersects the estimated $bedrock_{sp}$ reinforces our conclusion that data with relatively lower Mg/Ca and Sr/Ca ratios (Cluster 1) were less affected by PCP, and that Mg/Ca and Sr Ca altered by PCP evolved away from $bedrock_{sp}$, along the log-log slope (Fig. 4; Supplementary Fig. 3). Given the heterogeneity of the Tonasa Limestone[11], and the fact that Abadi Cave bedrock was collected ~250 m away from the stalagmites, it is remarkable that the measured bedrock Mg/Ca and Sr/Ca values are coherent with stalagmite values. It is possible that either Abadi Cave sits within a largely homogenous section of the Tonasa Limestone Formation, or a thick overhead bedrock and/or long drip pathways work to neutralise heterogeneities stemming from the surrounding limestone. Based on the GPS location of the cave entrance and satellite images of the terrain nearby, we estimate the overhead bedrock to be ~10-30 m thick. The occasional deviations in the Mg/Sr timeseries (even when PCP is operating) may be explained by changes in drip pathways and greater incorporation of bedrock heterogeneities.

Partition coefficients: E/Ca $bedrock_{sp}$

A wide range of calcite partition coefficients for Mg (Kd_{Mg}) and Sr (Kd_{Sr}) are reported in the literature from both laboratory[12–18] and cave studies[16,19–21]. The range of partition coefficients determined from these studies demonstrates that Kd_{Mg} and Kd_{Sr} depend on a variety of factors, including temperature and cave environment, dripwater composition, speleothem growth rates, and crystal surfaces.

Despite limited consensus, the Kd_{Mg} value of 0.031 (25°C) is fairly well-agreed on (e.g., Huang and Fairchild[16]; Sinclair et al.[22]; Tremaine and Froelich[20]). Additionally, Wassenburg et al.[21] defines Kd_{Mg} as a function of temperature, and arrived at essentially the same Kd_{Mg} value as Huang and Fairchild[16] (Kd_{Mg} = 0.0312 at 25°C). Without the ability to conduct a monitoring study at the Sulawesi cave site, Wassenberg's equation (Supplementary Equation 1) to calculate Kd_{Mg} for a range glacial-interglacial temperatures.

Supplementary Equation 1

$$Kd_{Mg} = 0.013 * e^{0.035*T}$$

Modern-day mean annual temperature in southwest Sulawesi (near sea level) is ~26.5°C. During glacial conditions, tropical sea-surface temperatures were ~3–4°C cooler than at present[23]. Therefore, to account for temperature-driven uncertainties in Kd_{Mg}, we include the temperature range between 22–27°C and estimate mean temperature for the G-I intervals covered by the Sulawesi stalagmites to be ~24°C (weighted towards cooler glacial conditions). Given the above, Abadi cave Kd_{Mg} = 0.030 and uncertainties range between 0.028 and 0.33.

Estimates of Kd_{Sr} vary widely in the literature because it is growth-rate dependent[12,15,24,25], influenced by the abundance of certain elements[13,21], and/or affected by crystal defects[14]. To determine an appropriate Kd_{Sr} value for Abadi Cave, we use the mathematical model of PCP from Sinclair et al.[22] (Supplementary Equation 2), where the linear slope of the ln(Sr/Ca) and ln(Mg/Ca) relationship is set by Mg and Sr partition coefficients.

Supplementary Equation 2

$$\frac{(Kd_{Sr} - 1)}{(Kd_{Mg} - 1)} = \text{PCP slope of ln(Sr/Ca) and ln(Mg/Ca)}$$

Using the Sinclair PCP slope of 0.88 ±0.13 and Kd_{Mg} = 0.030 (range between 0.028 and 0.33), we solve for Kd_{Sr} in Supplementary Equation 2 as follows:

$Kd_{sr} = [0.88 * (0.030 - 1)] + 1 = 0.15$

Lower $Kd_{sr} = [1.01 * (0.033 - 1)] + 1 = 0.02$

Upper $Kd_{sr} = [0.75 * (0.028 - 1)] + 1 = 0.27$

Thus, our estimate of Kd_{Sr} for Abadi Cave is 0.15 with a range between 0.02 and 0.27.

Supplementary Equation 3[20,26,27] below is used to determine the baseline elemental ratios in the Abadi Cave speleothems ($E/Ca\ bedrock_{sp}$), prior to the onset of PCP, based on Mg and Sr partition coefficients and bedrock solution chemistry alone ($E/Ca\ bedrock_{drip}$)

Supplementary Equation 3

$$E/Ca\ bedrock_{sp}\ (mmol/mol) = Kd_E * E/Ca\ bedrock_{drip}\ (mmol/mol)$$

For Mg/Ca, we apply the Kd_{Mg} = 0.030 (range 0.028–0.33) and a measured average Mg/Ca bedrock value of 12.453 (range 11.980 and 13.371 mmol/mol, n = 4). The resulting $bedrock_{sp}$ Mg/Ca value for speleothems is 0.375 mmol/mol with a range between 0.336 and 0.447 mmol/mol.

For Sr/Ca, we apply the Kd_{Sr} of 0.15 (range 0.02–0.27) and a measured average Sr/Ca bedrock value of 0.259 (range 0.237–0.279 mmol/mol, n = 4) for Abadi Cave. The resulting $bedrock_{sp}$ Sr/Ca value for speleothems is 0.038 mmol/mol with a range between 0.006 and 0.076 mmol/mol.

Mg/Ca and Sr/Ca cluster analysis and Sulawesi PCP slopes

K-means cluster analysis was performed on the four Sulawesi stalagmite Mg/Ca and Sr/Ca records to generate two groupings. Each data cluster is surrounded by an ellipse with 1.5 standard deviation (Supplementary Fig. 3). Cluster 1, containing lower Mg/Ca and Sr/Ca values, is interpreted to reflect data that have undergone limited PCP, whereas Cluster 2 contains higher values indicating the presence of PCP. Supplementary Figure 3 shows the distribution of the clusters for each stalagmite, log-log slopes, average Sulawesi PCP slope (0.82), calculated $bedrock_{sp}$, and measured Abadi cave bedrock. Due to variable growth rates and sampling resolutions across stalagmite records, the Mg/Ca and Sr/Ca data pairs are not evenly distributed. To ensure the raw sampling resolution is not significantly skewing the log-log slopes, regressions were performed on resampled data using the median resolution of the four Sulawesi records (81 years) and a low-resolution (1,000 years). All individual log-log slopes remain within error, regardless of sampling resolution (Supplementary Table 5). The intersection of the average Sulawesi PCP slope with the calculated $bedrock_{sp}$ (green circle, Supplementary Fig. 3) is the most likely value of $bedrock_{sp}$ for Abadi Cave, marking a 'starting point' for Mg/Ca and Sr/Ca to evolve away from as PCP progresses. The average PCP slope from the raw data resolution gives a predicted Abadi Cave $bedrock_{sp}$ value of Mg/Ca = 0.375 mmol/mol and Sr/Ca = 0.014 mmol/mol.

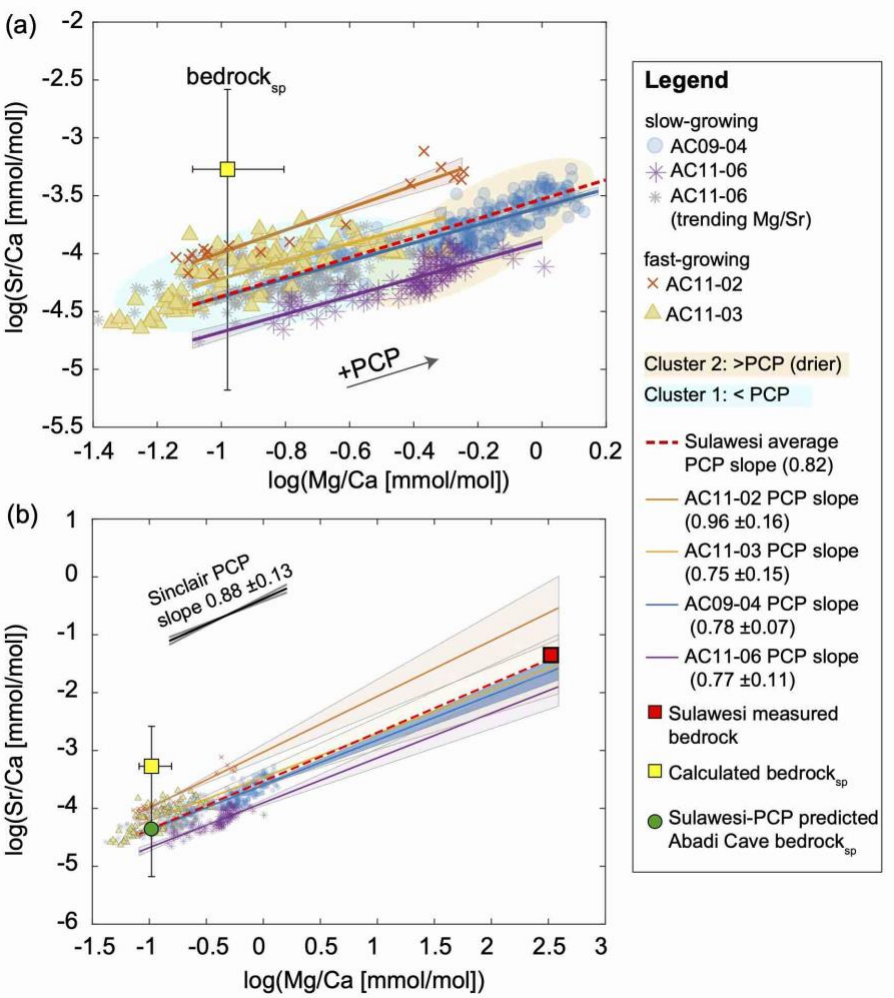

Supplementary Figure 3. Sulawesi Mg/Ca and Sr/Ca (original sampling resolution) log-log plots with PCP slopes and bedrock. (a) K-means cluster analysis and log-log plot of Mg/Ca and Sr/Ca data pairs. The regression slopes for each record are color-coded and intersect with bedrock$_{sp}$. The average Sulawesi PCP slope for raw data is 0.82 and shown by the red dashed line **(b)** Same as panel (a), but inluding measured Abadi bedrock (red square). The intersection of the average PCP slope with the calculated bedrock$_{sp}$ (green circle) is the most likely value of bedrock$_{sp}$ for Abadi Cave. The data-pairs in AC11-06 that do not have constant Mg/Sr (grey asterisks), and thus show limited PCP, are not included in the Sulawesi PCP regressions. K-means cluster analysis (kmeans clustering), ellipse determination (ELLIPSATE) and linear regression (Linear Regression plot with Confidence Intervals) were performed and plotted in Matlab (https://au.mathworks.com/matlabcentral/fileexchange/).

Timing of glacial-interglacial transitions

The timing of major glacial-interglacial transitions was determined using Bayesian change point methodology, this algorithm builds a linear regression model with 1000 iterations/sampled solutions to identify significant transitions and probabilities[28]. Supplementary Figure 4 shows change point analysis performed on normalised data for each Sulawesi stalagmite geochemical record ($\delta^{18}O$, Mg/Ca, and Sr/Ca) spanning the deglacial period. Although not identifiable as a significant change point, there is a slight increase in Mg/Ca approximately 1-2 ky earlier than the G-I shift in $\delta^{18}O$. This timing coincides with the initiation of increased growth rates in the fast-growing stalagmites as well as the final increases in atmospheric CO_2; these factors combined, as well as no corresponding shift

in $\delta^{18}O$, make it difficult to determine if this smaller transition indicates an early response to rainfall or a change in bedrock dissolution and elemental concentrations.

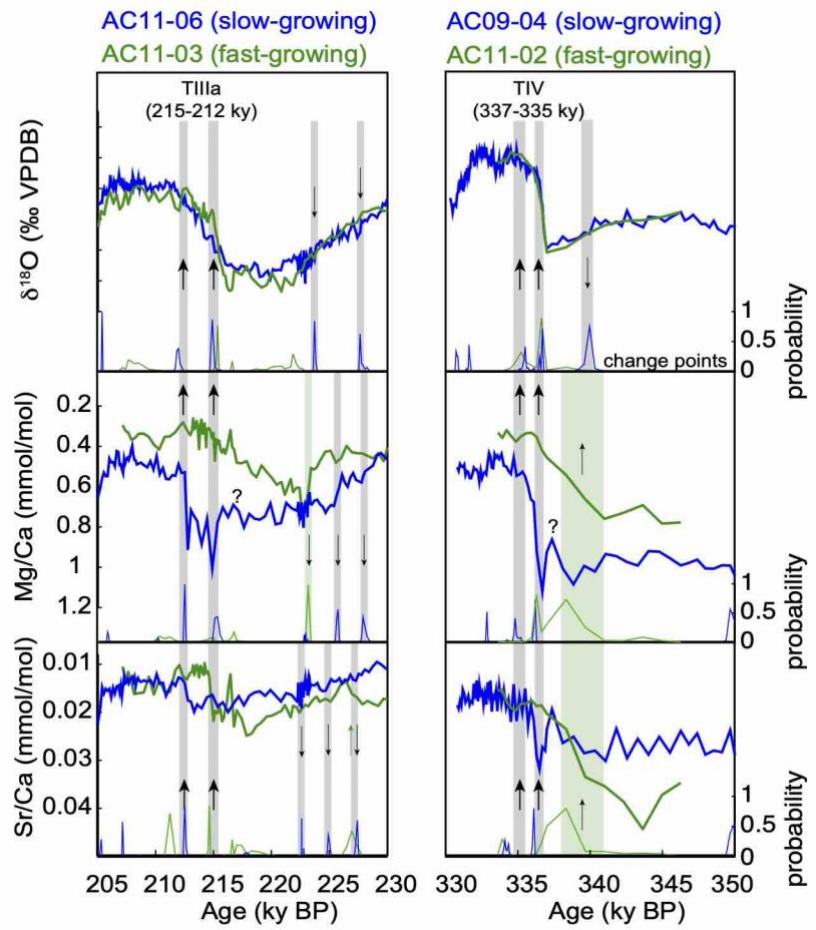

Supplementary Figure 4. Change point summary for Sulawesi stalagmite $\delta^{18}O$, Mg/Ca, and Sr/Ca. Results of change-point analysis with posterior probability estimates[28] for normalised d18O, Mg/Ca, and Sr/Ca timeseries for slow (blue) and fast-growing (green) sulawesi stalagmites. Grey vertical bars highlight shared major change points across the majority of records. Green vertical bars highlight change points primarily found in the fast-growin records. Arrows indicate the direction of change; large arrows are shown at G-I transition. The '?' notes a possible early decline in Mg/Ca for the slow-groing stalagmites, however there are no corresponding changepoints to suggest this is a significant transition.

The longer records from slow-growing stalagmites, AC11-06 and AC09-04, provide sufficient data prior to and following transitions to promote more reliable identification of significant changes. Cross-correlation analysis was used to further test the relationship between the Mg/Ca and $d^{18}O$ records across each deglacial transition for AC09-04 and AC11-06 (Supplementary Fig. 5). The deglacial intervals analysed span 220–210 ky BP for TIIIa, and 342–332 ky BP for TIV where PCP is clearly evident. Cross-correlation analysis was performed on Mg/Ca and $d^{18}O$ data pairs

interpolated to 100-year time intervals. The results confirm that the transition in Mg/Ca lags $\delta^{18}O$ by ~500-700 years for TIIIa and ~200 years for TIV.

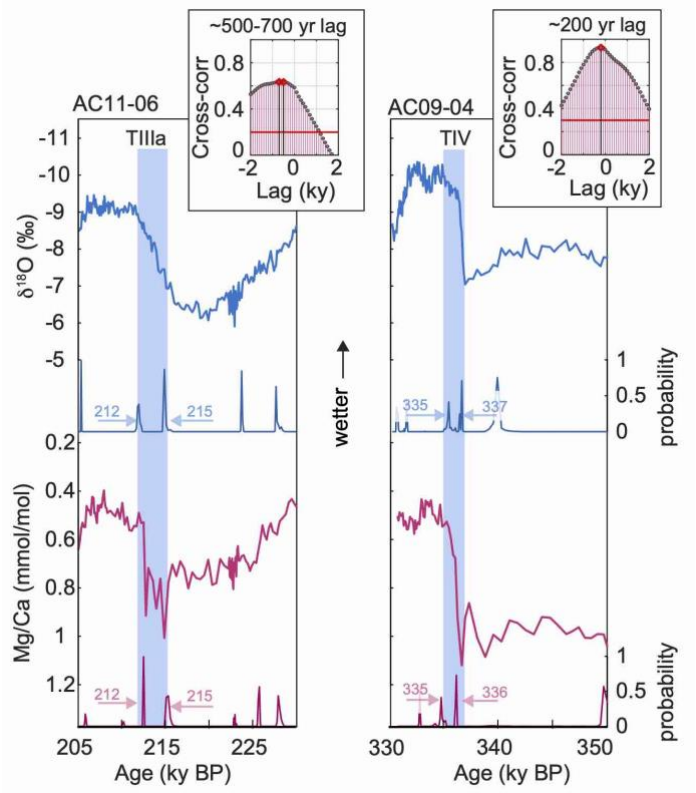

Supplementary Figure 5. TIIIa and TIV onset, conclusion, and cross-correlation in slow-growing Sulawesi stalagmite Mg/Ca and $\delta^{18}O$. Results of change-point analysis with posterior probability estimates[28] for the Mg/Ca and $\delta^{18}O$ timeseries for AC11-06 and AC09-04. Blue bars highlight $\delta^{18}O$ transitions based on the initiation of associated change points. The approximate timing of the change points and associated onset and conclusions of the terminations are annotated. Cross-correlation analysis is performed from 220 to 210 ky BP (TIIIa, AC11-06) and from 342 to 332 ky BP (TIV, AC09-04), to identify lead/lags that optimise correlation between Mg/Ca and $\delta^{18}O$ for each record (inset panels). The time-lags of Mg/Ca relative to $\delta^{18}O$ are shown in the upper right-side of each panel. Coss-correlations (crosscorr in Econometrics Toolbox) were performed using Matlab (https://es.mathworks.com/help/econ/crosscorr.html).

Supplementary References

1. Richards, D. A. & Dorale, J. A. Uranium-series chronology and environmental applications of speleothems. Rev. Mineral. Geochem. 52, 407–460 (2003).
2. Hellstrom, J. U–Th dating of speleothems with high initial ^{230}Th using stratigraphical constraint. Quat. Geochronol. 1, 289–295 (2006).
3. Scholz, D. & Hoffmann, D. ^{230}Th/U-dating of fossil corals and speleothems. Eiszeitalter Gegenwart Quat. Sci. J. 57, 52–76 (2008).
4. Dorale, J. A. et al. Uranium-series dating of speleothems: current techniques, limits, & applications. in Studies of Cave Sediments (eds. Sasowsky, I. D. & Mylroie, J.) 177–197 (Springer, Boston, MA, 2004).
5. Carolin, S. A. et al. Varied response of western Pacific hydrology to climate forcings over the last glacial period. Science 340, 1564–1566 (2013).
6. Kaufman, A. & Broecker, W. Comparison of Th^{230} and C^{14} ages for carbonate materials from lakes Lahontan and Bonneville. J. Geophys. Res. 70, 4039–4054 (1965).
7. Blaauw, M. & Christen, J. A. Flexible paleoclimate age-depth models using an autoregressive gamma process. Bayesian Anal. 6, 457–474 (2011).
8. McKay, N. P., Emile-Geay, J. & Khider, D. geoChronR – an R package to model, analyze, and visualize age-uncertain data. Geochronology 3, 149–169 (2021).
9. Bintanja, R., van de Wal, R. S. W. & Oerlemans, J. Modelled atmospheric temperatures and global sea levels

over the past million years. Nature 437, 125–128 (2005).
10. Schrag, D. P., Hampt, G. & Murray, D. W. Pore fluid constraints on the temperature and oxygen isotopic composition of the glacial ocean. Science 272, 1930–1932 (1996).
11. Wilson, M. E. J. & Bosence, D. W. J. The Tertiary evolution of South Sulawesi: a record in redeposited carbonates of the Tonasa Limestone Formation. Geol. Soc. London, Spec. Publ. 106, 365–389 (1996).
12. Lorens, R. B. Sr, Cd, Mn and Co distribution coefficients in calcite as a function of calcite precipitation rate. Geochim. Cosmochim. Acta 45, 553–561 (1981).
13. Mucci, A. & Morse, J. W. The incorporation of divalent Mg and divalent Sr into calcite overgrowths : influences of growth rate and solution composition. Geochim. Cosmochim. Acta 47, 217–233 (1982).
14. Pingitore, N. E. & Eastman, M. P. The coprecipitation of Sr^{2+} with calcite at 25°C and 1 atm. Geochim. Cosmochim. Acta 50, 2195–2203 (1986).
15. Tesoriero, A. J. & Pankow, J. F. Solid solution partitioning of Sr^{2+}, Ba^{2+}, and Cd^{2+} to calcite. Geochim. Cosmochim. Acta 60, 1053–1063 (1996).
16. Huang, Y. & Fairchild, I. J. Partitioning of Sr2+ and Mg2+ into calcite under karst-analogue experimental conditions. Geochim. Cosmochim. Acta 65, 47–62 (2001).
17. Gabitov, R. I. & Watson, E. B. Partitioning of strontium between calcite and fluid. Geochemistry, Geophys. Geosystems 7, 1–12 (2006).
18. Day, C. C. & Henderson, G. M. Controls on trace-element partitioning in cave-analogue calcite. Geochim. Cosmochim. Acta 120, 612–627 (2013).
19. Gascoyne, M. Trace-element partition coefficients in the calcite-water system and their paleoclimatic significance in cave studies. J. Hydrol. 61, 213–222 (1983).
20. Tremaine, D. M. & Froelich, P. N. Speleothem trace element signatures: A hydrologic geochemical study of modern cave dripwaters and farmed calcite. Geochim. Cosmochim. Acta 121, 522–545 (2013).
21. Wassenburg, J. A. et al. Calcite Mg and Sr partition coefficients in cave environments: Implications for interpreting prior calcite precipitation in speleothems. Geochim. Cosmochim. Acta 269, 581–596 (2020).
22. Sinclair, D. J. et al. Magnesium and strontium systematics in tropical speleothems from the Western Pacific. Chem. Geol. 294, 1–17 (2012).
23. Lea, D. W., Pak, D. K. & Spero, H. J. Climate Impact of Late Quaternary Equatorial Pacific Sea Surface Temperature Variations. Science 289, 1719–1724 (2000).
24. Tang, J., Köhler, S. J. & Dietzel, M. Sr^{2+}/Ca^{2+} and $^{44}Ca/^{40}Ca$ fractionation during inorganic calcite formation: I. Sr incorporation. Geochim. Cosmochim. Acta 72, 3718–3732 (2008).
25. Gabitov, R. I., Sadekov, A. & Leinweber, A. Crystal growth rate effect on Mg/Ca and Sr/Ca partitioning between calcite and fluid: An in situ approach. Chem. Geol. 367, 70–82 (2014).
26. Henderson, L. M. & Kracek, F. C. The fractional precipitation of barium and radium chromates. J. Am. Chem. Soc. 49, 738–749 (1927).
27. Morse, J. W. & Bender, M. L. Partition coefficients in calcite: Examination of factors influencing the validity of experimental results and their application to natural systems. Chem. Geol. 82, 265–277 (1990).
28. Ruggieri, E. A Bayesian approach to detecting change points in climatic records. Int. J. Climatol. 33, 520–528 (2012).